

# *Ab initio* $^1A'$ ground potential energy surface and transition state theory kinetics study of the $O(^1D) + N_2O \rightarrow 2NO$ , $N_2 + O_2(a^1\Delta_g)$ reactions

Miguel González<sup>a)</sup> and Rosendo Valero

*Departament de Química Física i Centre de Recerca en Química Teòrica, Universitat de Barcelona. C/Martí i Franquès, 1. 08028 Barcelona, Spain*

Josep Maria Anglada

*Institut d'Investigacions Químiques i Ambientals de Barcelona, CID-CSIC. C/Jordi Girona, 18-26. 08034 Barcelona, Spain*

R. Sayós<sup>b)</sup>

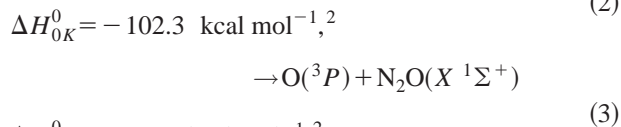
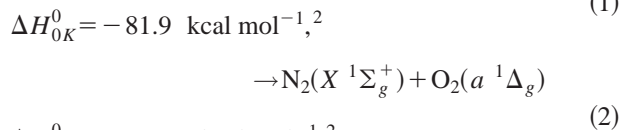
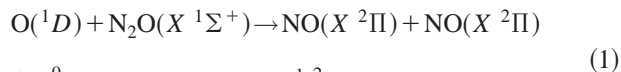
*Departament de Química Física i Centre de Recerca en Química Teòrica, Universitat de Barcelona. C/Martí i Franquès, 1. 08028 Barcelona, Spain*

(Received 27 April 2001; accepted 10 July 2001)

An *ab initio* study of the  $^1A'$  ground potential energy surface (PES) of the  $O(^1D) + N_2O(X^1\Sigma^+)$  system has been performed at the CASPT2//CASSCF (complete active space second-order perturbation theory//complete active space self-consistent field) level with Pople basis sets. The two reactions leading to  $2NO(X^2\Pi)$  [reaction (1)] and  $N_2(X^1\Sigma_g^+) + O_2(a^1\Delta_g)$  [reaction (2)] products have been investigated. In both reactions a *trans*-approach of the attacking oxygen to the  $N_2O$  moiety is found to be preferred, more markedly in reaction (1). For this reaction also a *cis*-path is feasible and is possibly connected with the *trans*-path by a transition state placed below reactants. A thorough characterization of the entrance zone has been performed to allow for subsequent kinetics calculations. Fixed angle and minimum energy paths have been constructed and transition state geometries have been refined at the CASPT2 level, thus obtaining approximate structures and frequencies for the latter. From these calculations it can be inferred that both reactions proceed without an energy barrier. Rate constant calculations in the 100–1000 K temperature range based on CASPT2 structures and using the transition state theory yield values in good agreement with experiment for the two reactions, especially when a proper scaling of the energy barriers is performed. Also, for comparative purposes quasiclassical trajectory calculations were performed on reaction (1) in the same temperature range, using a previous pseudotriatomic analytical potential energy surface, obtaining good agreement with experiment. © 2001 American Institute of Physics. [DOI: 10.1063/1.1398101]

## I. INTRODUCTION

The reaction of  $N_2O$  with  $O(^1D)$  is considered to be the main source of stratospheric  $NO$ ,<sup>1</sup> which plays a relevant role in the natural degradation of ozone. The  $O(^1D) + N_2O$  reaction presents the following reaction channels:



Most studies on the  $O(^1D) + N_2O$  reaction have been devoted to the study of reaction (1), due to its particular interest and also because it is easier to study at the laboratory

than the other reactions. The rate constants for reactions (1)–(3) have been measured in the 200–350 K temperature interval, their recommended values being, respectively,  $7.2 \times 10^{-11}$ ,  $4.4 \times 10^{-11}$ , and  $< 1 \times 10^{-12} \text{ cm}^3 \text{ molecule}^{-1} \text{ s}^{-1}$ .<sup>3</sup> Hence, in thermal conditions reactions (1) and (2) are very fast with  $k_1/k_2 = 1.6$ , and the electronic quenching process is negligible with respect to both reactions. The  $NO(v')$  vibrational distribution has been measured in different  $v'$  intervals.<sup>4–11</sup> With the exception of Refs. 5 and 8–9, the experiments were done under  $NO$  rotational relaxation conditions. The  $NO$  rotational distribution has been reported for some vibrational levels.<sup>5,8,9,12,13</sup> The stereodynamics of reaction (1) has been explored in Doppler-resolved polarized laser-induced fluorescence (LIF) experiments<sup>5,8,9,12–14</sup> probing some specific  $NO$  rovibrational levels. The rovibrational distributions of the  $NO$  molecules arising from the half-reaction  $O(^1D) \cdot N_2O$  have also been reported.<sup>15</sup>

This system has been the object of several theoretical investigations. *Ab initio* calculations of the ground  $^1A'$  potential energy surface (PES) using the Møller–Plesset<sup>16</sup> and Brueckner<sup>17</sup> methods, and density functional theory (DFT) calculations<sup>17,18</sup> have been reported. Also, a multiconfigura-

<sup>a)</sup>Electronic mail: miguel@qf.ub.es

<sup>b)</sup>Electronic mail: r.sayos@qf.ub.es

tional study on the ground and first excited PESs has been published.<sup>19</sup> Quasiclassical trajectory (QCT) studies<sup>6,20–22</sup> on the dynamics of reaction (1) have been carried out, mainly at a triatomic level and employing LEPS (London-Eyring-Polanyi-Sato) empirical PESs.<sup>20–22</sup> QCT vibrational distributions of reactions (1) and (2) have been derived<sup>6</sup> using an empirical PES<sup>23</sup> that describes the four-atom system. Previous work focusing on some selected portions of the PES also exists. In particular, *ab initio*<sup>24,25</sup> and DFT studies<sup>26,27</sup> have been devoted to the characterization of the (NO)<sub>2</sub> van der Waals (vdW) dimers. These dimers have been experimentally detected in *cis*-<sup>28–31</sup> and *trans*-conformations.<sup>31,32</sup> A detailed comparison between the theoretical and experimental data available on the (NO)<sub>2</sub> dimers can be found in Ref. 25. High-energy N<sub>2</sub>O<sub>2</sub> isomers (about 40–80 kcal mol<sup>-1</sup> above NO+NO) with potential applications in the field of high-impulse fuels have been investigated. There is some indirect experimental evidence on the existence of this kind of isomers, which could be involved in reactions such as O(<sup>3</sup>P, <sup>1</sup>D)+N<sub>2</sub>O or N(<sup>2</sup>D, <sup>2</sup>P)+NO<sub>2</sub>. A certain number of *ab initio* investigations aimed at the elucidation of their structures and energetics have been carried out.<sup>33–38</sup>

The main goal of this work is to characterize the ground PES of the system O(<sup>1</sup>D)+N<sub>2</sub>O(X <sup>1</sup>Σ<sup>+</sup>) with high-level *ab initio* methods, in order to obtain in the near future an analytical representation of the PES suitable to perform dynamics studies. This work is organized as follows. In Sec. II we discuss in some detail the selection of the *ab initio* methods and basis sets employed. Section III describes the stationary points and the comparison with previous theoretical and experimental works. In Sec. IV rate constant calculations based on the conventional transition state theory are put forward and compared with experiment. Finally, the summary and conclusions are given in Sec. V.

## II. SELECTION OF THE METHOD

The selection of the computational methods employed has been guided by the nature of the system under study. An important feature of the O(<sup>1</sup>D)+N<sub>2</sub>O system is its diradical character, particularly in the entrance [owned to the O(<sup>1</sup>D) species] and exit zones [owned to the NO(X <sup>2</sup>Π) and O<sub>2</sub>(a <sup>1</sup>Δ<sub>g</sub>) species]. Therefore, in a qualitatively correct approach one must, in general, keep at least two configurations<sup>39</sup> throughout the PES. However, as a first approximation, we have used several DFT functionals as implemented in the GAUSSIAN 94 package of programs<sup>40</sup> at the unrestricted level of theory, thereby generating a broken symmetry (in spin and space) singlet wave function.<sup>41</sup> The results obtained in this way,<sup>18</sup> which are not presented in this work, are reasonable in those zones of the PES where the wave function of the system can be approximated by a unique closed-shell configuration (intermediate zones which present a strong chemical interaction). However, they are considerably in error in the entrance and exit zones, where the spin contamination is increasingly important towards reactants and products. It is well known that, for symmetry broken solutions in singlet diradicals, the calculated state is essentially an equally weighted mixing of the ground open-shell singlet and triplet states, the mean-square value of the

total spin ( $\langle S^2 \rangle$ ) being equal to 1.0 in atomic units. One could improve the wave function to some extent by projecting out the triplet component, but there is no such a procedure available in GAUSSIAN 94 for DFT calculations, making it necessary to correct for it manually (see, e.g., the method outlined in Ref. 42). In this way, we do not expect to obtain, for example, transition states accurate enough for our purposes, because the shape of the PES for geometries close to them has a strong influence on the kinetics. Hence, a multi-configurational method should be required to reach a correct description of this system.

For the reasons stated above, we have adopted the CASPT2//CASSCF (complete active space second-order perturbation theory//complete active space self-consistent field) method. Thus, we have obtained the optimal geometries at the CASSCF level<sup>43</sup> and performed CASPT2<sup>44,45</sup> point-wise calculations on the resulting structures. This approach seems to be adequate, since the multiconfigurational CASSCF method provides the basis for an accurate description of bond breaking and forming processes, and can treat on an equal footing the ground and excited states. Moreover, this method is intended to introduce the main part of the nondynamical correlation energy.<sup>43</sup> The CASPT2 method is based on the calculation of the energy at the second order of perturbation theory, taking as the zeroth-order wave function the one resulting from the CASSCF step, thus introducing the dynamical correlation.<sup>44,45</sup> This method is not supposed to shift to a great extent the geometries obtained at the CASSCF level (see below to clarify this point). The combined CASPT2//CASSCF method has an estimated error in the exoergicities of  $\pm 2$  kcal mol<sup>-1</sup> for isogyric reactions (i.e., reactions that conserve the number of electron pairs in reactants and products), assuming that the active space includes all the valence electrons and a large enough basis set has been used.

Two standard Cartesian Gaussian basis sets of Pople and co-workers<sup>46–48</sup> have been used: the 6-31G(*d*) basis set, comprising 60 contracted basis functions for the N<sub>2</sub>O<sub>2</sub> system, and the 6-311G(2*d*) basis set, which amounts to 100 contracted basis functions. The first basis set has been used mainly to perform the initial searches and the second one to obtain the final structures, harmonic vibrational frequencies, and energies. The 6-311G(2*d*) basis set has been considered to be of enough quality because it yields good values of exoergicities (see below) and a rather correct description of the demanding vdW (NO)<sub>2</sub> dimer properties.<sup>25</sup> Therefore, from now on we will drop the basis set when referring to the methods applied. All the stationary points were characterized as either minima (MINs) or transition states (TSs) calculating their corresponding harmonic vibrational frequencies. The G2 variant of the CASPT2 method has been employed, because it gives slightly better values of the exoergicities than the standard and other nonstandard variants. The calculations were performed by means of the MOLCAS 4.1<sup>49</sup> package of programs.

A crucial aspect in the CASSCF method is the selection of the active space, to which different approaches can be found in the literature.<sup>50–52</sup> We have first followed the method described in Ref. 51, i.e., by performing a previous

TABLE I. Reaction energies and N<sub>2</sub>O geometry with different chosen active spaces. The active spaces are defined as indicated in the text.

Reaction <sup>a</sup>		(14,12) <sub>A</sub>	(14,12) <sub>B</sub>	(18,14) <sub>A</sub>	(18,14) <sub>B</sub>	Experiment
O( <sup>1</sup> D)+N <sub>2</sub> O→NO+NO	(1)	-76.1 (-79.7)	-93.1 (-82.4)	-78.3 (-80.5)	-80.0 (-81.0)	-80.4
O( <sup>1</sup> D)+N <sub>2</sub> O→N <sub>2</sub> +O <sub>2</sub> ( <i>a</i> <sup>1</sup> Δ <sub>g</sub> )	(2)	-100.8 (-103.8)	-117.8 (-106.4)	-101.3 (-103.6)	-103.0 (-104.0)	-100.9

	R <sub>NN</sub> /Å	R <sub>NO</sub> /Å	<NNO/°
N <sub>2</sub> O <sup>b</sup>	1.1323/1.1146 (1.1343/1.1339)[1.1273]	1.1901/1.1949 (1.1931/1.1919)[1.1851]	180.0/180.0 (180.0/180.0)[180.0]

<sup>a</sup>Energies in kcal mol<sup>-1</sup>. Both the A- and B-type active spaces given refer to reactants, while B-type active spaces were always employed in products. In parentheses are given the values derived from point-wise CASPT2 calculations in optimal CASSCF geometries. Experimental energies derived from Refs. 54–57.

<sup>b</sup>Geometries correspond to: (14,12)<sub>A</sub>/(14,12)<sub>B</sub> and, in parentheses, (18,14)<sub>A</sub>/(18,14)<sub>B</sub>. Experimental geometry (in brackets) taken from Ref. 57.

SCF MO-based MRCI calculation on each one of the previously obtained DFT stationary points, diagonalizing the spin-averaged first-order density matrix, and keeping as active those molecular orbitals (MOs) bearing natural orbital occupation numbers (NOONs) within the limits 0.02–1.98. This method relies on the fact that these occupations are essentially maintained in the CASSCF wave function. Occupations off the above-indicated limits can originate, e.g., convergence problems, a not clear-cut definition of the orbitals as either active or inactive, and difficulties in the delimitation of the nondynamical/dynamical correlation. There are suggestions<sup>50</sup> that, choosing the active orbitals in this way, one obtains at a single point of the PES the lowest energy for a given size of the CI expansion (i.e., for a fixed number of active electrons and MOs).

In our case, the application of the NOONs criterion leads to a different active space for each one of the two reactive channels, i.e., 14 electrons in 12 orbitals [or (14,12)] for reaction (1) and 12 electrons in 10 orbitals [or (12,10)] for reaction (2). Thus, it is inconsistent in, for example, reactants. This problem can be overcome by taking a homogeneous active space for the whole PES, even when the NOONs are not strictly in keeping with the above-mentioned criterion. Nevertheless, since we focus here on the ground PES rather than in a balanced description of all the singlet PESs of the system, we have tried to obtain the lowest-energy stationary points on the ground PES, which would be almost equivalent to obtaining the set of NOONs maximally different from 2.0 or 0.0, but not necessarily within the limits 1.98–0.02 (more details about this point can be found, e.g., in Ref. 53). This is further justified by the absence of analytical gradients at the CASPT2 level in MOLCAS 4.1, thus being necessary to obtain CASSCF geometries of as good a quality as possible. We note that this has been done at the cost of dealing with active spaces which are not strictly homogeneous throughout the PES.

According to the former, and since at present it is not feasible for this system to include all the valence electrons as active, some trial and error was necessary in order to obtain the set of active MOs giving the lowest-energy CASSCF stationary points. In this respect, a comparison with experimental results was found to be necessary.

Regarding this question, it is worth presenting an outline of the PESs arising from the O(<sup>1</sup>D)+N<sub>2</sub>O(X<sup>1</sup>Σ<sup>+</sup>) system. The <sup>1</sup>D<sub>g</sub> state of oxygen is five-fold degenerate, and a Car-

tesian basis set for its representation in the cubic O<sub>h</sub> group can be chosen as follows:  $x^2-z^2$ ,  $xy$ ,  $xz$ ,  $yz$ , and  $3y^2-r^2$ . In this basis the resolution of the <sup>1</sup>D<sub>g</sub> state into the species of the C<sub>s</sub> subgroup ( $xy$  symmetry plane) leads to three <sup>1</sup>A' ( $x^2-z^2$ ,  $xy$ , and  $3y^2-r^2$ ) and two <sup>1</sup>A'' ( $xz$  and  $yz$ ) states. An analogous description of the <sup>1</sup>D<sub>g</sub> state can be effected by considering the three valence Cartesian ( $2p_x$ ,  $2p_y$ ,  $2p_z$ ) orbitals of the oxygen atom and performing the replacements  $x \rightarrow 2p_x$ ,  $y \rightarrow 2p_y$ ,  $z \rightarrow 2p_z$ . In this way, it is evident that for the first two <sup>1</sup>A' components only two  $2p$  oxygen atomic orbitals are involved, but in the third one ( $3y^2-r^2$ ) all three  $2p$  orbitals are required. From the above-mentioned states, two <sup>1</sup>A' and two <sup>1</sup>A'' correlate with the products of reaction (1), and only one <sup>1</sup>A' and one <sup>1</sup>A'' correlate with those of reaction (2). Hence, in C<sub>s</sub> symmetry only one <sup>1</sup>A' and one <sup>1</sup>A'' PESs correlate reactants and both kinds of products. In this work we are concerned with the lowest-energy <sup>1</sup>A' PES, which also corresponds to the ground PES of the system.

We have chosen two active spaces: the first one includes all the atomic  $2p$ -derived molecular orbitals and, optionally, one of them has been replaced by one  $2s$  (N atom)-derived MO (spaces B and A, respectively; see below). Hence, 14 electrons in 12 orbitals [(14,12) hereafter] are introduced. In the second one, 4 additional electrons occupying two  $2s$  (N and O atoms)-derived MOs are added to either (14,12) A or B, summing up to 18 electrons in 14 orbitals [we will indicate these active spaces by (18,14)<sub>A</sub> and (18,14)<sub>B</sub>, respectively]. The size of the CI expansion is of about 85 000 and 500 000 configuration state functions (CSFs) for the <sup>1</sup>A' symmetry and the (14,12) and (18,14) active spaces, respectively. The need to enlarge further the already extensive (14,12) active space will be discussed in Sec. III.

In Table I are shown the energies of reactions (1) and (2), and the N<sub>2</sub>O geometry for the (14,12) and (18,14) active spaces. It is remarkable the variation in the exoergicities and N<sub>2</sub>O geometry (NN distance) between sets A and B, particularly for the CASSCF(14,12) calculations in which space A is clearly favored. The energy differences are much smaller for the (18,14) active space. When CASPT2 point-wise calculations are performed, all the active spaces [either (14,12) or (18,14)] tend to give similar results. The need of correlating one  $2s$  N<sub>2</sub>O MO could be expected because it is known that nitrogen is a limiting case with respect to the type of orbitals to be chosen as active.<sup>44</sup> The almost double occu-

pancy of the atomic oxygen  $2p_y$  orbital in the very entrance zone (reactants and vdW entrance minimum) is owed to the fact that for the  $(14,12)_A$  space the ground PES correlates with the  $x^2-z^2$  component of  $O(^1D)$ , thus being preferred to the  $(14,12)_B$  description ( $3y^2-r^2$  component). Both components are degenerate and, therefore, the energy difference between both active spaces stems from the inclusion of an atomic nitrogen  $2s$  orbital in space  $A$ , thus allowing for a better description of the  $N_2O$  fragment. For the  $(18,14)$  active space, the differences are relatively minor, because a larger portion of the nondynamical correlation has been introduced. However, the lowest-energy criterion seems to favor  $(18,14)_A$  in reactants and the very entrance zone. The  $(18,14)_A$  space also leads to the partition  $O(2,2) + N_2O(16,12)$ ; that is, the full valence space is correlated in  $N_2O$ . The intermediate and exit zones in reaction (1) are better described by the  $(14,12)_B$  and  $(18,14)_B$  spaces. For reaction (2) the optimal active space, which is essentially of type  $A$  in reactants and  $B$  otherwise, changes slightly from one stationary point to another. This was to be expected since we are interested in finding the lowest-energy CASSCF profile and the full-valence active space is not feasible.

Bearing all this in mind, we decided to employ the  $A$ -type spaces in the very entrance zone and the  $B$ -type ones in the rest of the PES. Hence, the geometrical optimization and characterization of the stationary points on the PES was performed at the CASSCF(14,12) level. These structures were then reoptimized at the CASSCF(18,14) level. Further, in some relevant zones of the PES systematic scans were carried out yielding several candidates to stationary points. For some of them, the minimization of the gradient led to the location of new structures, for which the harmonic vibrational frequencies were also calculated (see below).

### III. *Ab initio* results

#### A. CASSCF stationary points

The geometries (CASSCF), harmonic vibrational frequencies (CASSCF), and energies (CASSCF and CASPT2) of the stationary points of reactions (1) and (2), obtained employing the  $(14,12)$  and  $(18,14)$  active spaces, are shown in Tables II, III, and IV, respectively. The ground PES will also be analyzed in terms of electronic configurations and predominant CSFs, as well as the nature of the bonding, for each one of the stationary points found. Thus, the main electronic configurations of the stationary points at the CASSCF(18,14) level are presented in Table V. Schematic representations of the minimum energy reaction paths (MERP) of reactions (1) and (2) are presented in Figs. 1 and 2, respectively. In what follows, the results obtained will also be compared with previously reported data.

The harmonic frequencies have been calculated numerically only at the CASSCF(14,12) level because the CASSCF(18,14) calculations are computationally very expensive (Table III). For MIN  $B1$  and TS  $B1$  the frequencies are calculated at the CASSCF(18,14) level, but the out-of-plane normal modes, that keep  $C_2$  symmetry, must be calculated separately (cf. Table III). This is due to limitations in the MOLCAS 4.1 program, as  $(18,14)$  calculations are too large

to be performed in  $C_1$  symmetry. For the same reason, in TS  $E1$  only four frequencies can be calculated; the remaining two, which are of  $C_1$  symmetry, cannot even be calculated with the available software.

The connections between the TSs and MINs for reaction (1) (Fig. 1) and reaction (2) (Fig. 2) have been checked by the nature of the TS imaginary mode and full optimization departing from geometries obtained from small distortions of the TS structures. As is apparent in Table IV, the qualitative character of the PES varies considerably when moving from the CASSCF to the CASPT2 method. There is a general stabilization of the stationary points and, in particular, the marked decrease in the barrier heights for the entrance zone suggests that no CASPT2 transition states exist in this zone, and that no stationary points at all may exist in reaction (2) (note the steady decrease in CASPT2 energy towards products). Besides, there is an acute variation in the geometries of the stationary points in the exit zone, i.e., shortening of the NN distance and stabilization of the  $(NO)_2$  vdW minima;<sup>25</sup> the same tendency is to be expected in the very entrance zone. All these aspects will be considered in more detail in what follows when considering the stationary points of each reaction.

This evidence suggests that including dynamical correlation is of utmost importance for predicting the energies and structures of the  $N_2O_2$  system, particularly in the entrance and exit zones. The entrance zone determines the energy and geometry of the TSs, which are supposed to yield an almost null barrier. Thus, a good prediction of the rate constants by means of more accurately obtained TSs would support the feasibility of the CASPT2//CASSCF approach as a means of studying the whole ground  $^1A'$  PES of the system (see Secs. III C and IV).

The reaction energies are shown in Table IV (see also Figs. 1 and 2). The exoergicities of reactions (1) and (2), which were partially discussed in Sec. II regarding the selection of the active space, are in good agreement with experiment (Table IV). At the highest level considered, i.e., CASPT2//CASSCF(18,14) with zero-point energy (ZPE) included, the exoergicity of reaction (1) is in almost perfect agreement with experiment (0.1 kcal mol<sup>-1</sup> deviation), whereas for reaction (2) it is overestimated by 2.9 kcal mol<sup>-1</sup>. Although the second value is somewhat larger than the accuracy of the method, these can be considered as very good results, since not all the valence MOs are correlated and the basis set is of a moderate size.

Regarding the MERP of reaction (1), as it can be seen in Fig. 1, it corresponds to a *trans*-MERP, placed energetically below reactants (including the ZPE), in which the  $O(^1D)$  atom attacks the terminal N atom of the  $N_2O$  molecule forming an entrance channel vdW minimum [MIN  $A1$  ( $^1A', C_s$ )]. This structure evolves through TS  $A1$  ( $^1A', C_s$ ) to MIN  $B1$  ( $^1A_g, C_{2h}$ ), bearing a double bond between the nitrogen atoms. The double bond breaks on elongation of the NN distance, giving rise to TS  $B1$  ( $^1A_g, C_{2h}$ ), and leading to the *trans*- $(NO)_2$  vdW dimer [MIN  $C1$  ( $^1A_g, C_{2h}$ )] in the exit zone, and finally to products (2 NO). This MERP can be summarized as follows:  $O(^1D) + N_2O$

TABLE II. Geometries of the stationary points at the CASSCF(18,14) level. The CASSCF(14,12) geometries are shown in parentheses, with the exception of MIN *B1*, TS *B1*, and TS *E1* (see the text). The available experimental data are given in brackets.

Stationary point	$R_{NN}/\text{\AA}$	$R_{NO}/\text{\AA}$	$R_{OO}/\text{\AA}$	$\angle NNO/^\circ$	$\angle NNO/^\circ$	Dihedral/ $^\circ$ <sup>aa</sup>
O( <sup>1</sup> <i>D</i> )+N <sub>2</sub> O <sup>b</sup>	1.1343 (1.1323) [1.1273]	1.1931 (1.1901) [1.1851]		180.0 (180.0) [180.0]		
NO+NO <sup>c</sup>		1.1605 (1.1586) [1.1508]				
N <sub>2</sub> +O <sub>2</sub> ( <i>a</i> <sup>1</sup> $\Delta_g$ ) <sup>c</sup>	1.1045 (1.1037) [1.0977]		1.2332 (1.2332) [1.2156]			
Reaction (1)						
MIN <i>A1</i>	1.1342 (1.1323)	1.1929,3.3975 (1.1898,3.3974)		179.9,169.1 (180.0,169.1)		180.0 (180.0)
TS <i>A1</i>	1.1314 (1.1371)	1.1875,1.9408 (1.1799,1.7641)		178.3,151.3 (176.7,128.1)		180.0 (180.0)
MIN <i>B1</i>	1.2700	1.2099,1.2099		137.7,137.7		180.0
TS <i>B1</i>	1.4578	1.1892,1.1892		129.5,129.5		180.0
MIN <i>C1</i>	3.5403 (3.6128)	1.1604,1.1604 (1.1585,1.1585)		109.1,109.1 (109.3,109.3)		180.0 (180.0)
TS <i>C1</i>	3.5293 (3.5291)	1.1606,1.1606 (1.1586,1.1586)		91.0,91.0 (91.0,91.0)		57.8 (57.8)
MIN <i>D1</i> <sup>d</sup>	3.0623 (3.3109) [2.2630]	1.1603,1.1603 (1.1585,1.1585) [1.1515,1.1515]		90.8,90.8 (86.9,86.9) [97.2,97.2]		0.0 (0.0) [0.0]
TS <i>E1</i> <sup>e</sup>	1.2471	1.3372,1.3372		108.7,108.7		11.9
MIN <i>E1</i>	1.2618 (1.2653)	1.4052,1.4052 (1.4001,1.4001)		94.8,94.8 (94.9,94.9)		0.0 (0.0)
TS <i>F1</i>	1.2379 (1.2800)	1.3498,1.3498 (1.3402,1.3402)		109.7,109.7 (104.5,104.5)		0.0 (14.8)
Reaction (2)						
MIN <i>A2</i>	1.1339 (1.1320)	1.1931 (1.1900)	3.3541 (3.3541)	179.9 (179.9)	76.4 (76.3)	180.0 (180.0)
TS <i>A2</i>	1.1272 (1.1236)	1.2099 (1.2114)	1.9038 (1.8623)	179.1 (179.8)	103.3 (101.2)	180.0 (180.0)
MIN <i>B2</i>	1.1199 (1.1169)	1.2340 (1.2337)	1.6228 (1.6148)	178.2 (179.5)	102.5 (101.0)	180.0 (180.0)
TS <i>B2</i>	1.1151 (1.1125)	1.3751 (1.3729)	1.4469 (1.4461)	172.9 (171.5)	106.5 (106.3)	0.0 (0.0)
Reactions (1)–(2) connection						
TS <i>A3</i>	(1.1991)	(1.4147)	(1.4988)	(110.0)	(97.8)	(18.8)

<sup>a</sup>Dihedral angle is defined as  $\angle ONNO$  for reaction (1) and  $\angle NNOO$  for reaction (2).

<sup>b</sup>Experimental data taken from Ref. 57.

<sup>c</sup>Experimental data taken from Ref. 55.

<sup>d</sup>Experimental data taken from Ref. 28.

<sup>e</sup>The gradient norm ( $\sim 7 \times 10^{-3}$  a.u.) is larger than for the remainder of the stationary points, for which it is  $< 10^{-4}$  a.u.

$\rightarrow$ MIN *A1*  $\rightarrow$ TS *A1*  $\rightarrow$ MIN *B1*  $\rightarrow$ TS *B1*  $\rightarrow$ MIN *C1*  $\rightarrow$ 2 NO.

There is an alternative path (*trans/cis*-MERP), with higher energetic requirements than the *trans*-one, but which is also situated energetically below reactants (Fig. 1). The initial part of the *trans/cis*-MERP is identical to that of the *trans*-MERP, but it changes after MIN *B1* (*trans*-conformation), passes over an interconversion barrier [TS *E1* (<sup>1</sup>*A*, *C*<sub>2</sub>)], and connects with the cyclic MIN *E1* (<sup>1</sup>*A*<sub>1</sub>, *C*<sub>2v</sub>) that has a *cis*-conformation. This minimum may evolve through TS *F1* (<sup>1</sup>*A*<sub>1</sub>, *C*<sub>2v</sub>), which connects with the *cis*-(NO)<sub>2</sub> vdW dimer [MIN *D1* (<sup>1</sup>*A*<sub>1</sub>, *C*<sub>2v</sub>)], and then with products. This MERP from MIN *B1* can be summarized as

follows: MIN *B1*  $\rightarrow$ TS *E1*  $\rightarrow$ MIN *E1*  $\rightarrow$ TS *F1*  $\rightarrow$ MIN *D1*  $\rightarrow$ 2 NO. The transition states TS *C1* (<sup>1</sup>*A*, *C*<sub>2</sub>) connects both types of (NO)<sub>2</sub> vdW dimers.

The present *ab initio* results show that for reaction (1) there is not an energy barrier (including the ZPE) above reactants. According to this, high rate constant values, with a slight dependence on the temperature, may be expected for this reaction, as has actually been found experimentally.<sup>3</sup>

Regarding the main electronic configurations of the stationary points (Table V), we first note that each electronic configuration corresponds to a single closed-shell CSF. Hence, in reactants two equal-weighted CSFs are required to describe the  $x^2-z^2$  component of the <sup>1</sup>*D*<sub>g</sub> diradical state.

TABLE III. Harmonic vibrational frequencies (in  $\text{cm}^{-1}$ ) of the stationary points at the CASSCF(14,12) level. The symmetries of the normal vibrational modes are given in parentheses, and the available experimental data are given in brackets. For the MIN *B1* and TS *B1* stationary points the harmonic vibrational frequencies have been calculated at the CASSCF(18,14) level (see the text).

Stationary point	$\omega_1$	$\omega_2$	$\omega_3$	$\omega_4$	$\omega_5$	$\omega_6$	ZPE/kcal mol <sup>-1</sup>
O( <sup>1</sup> <i>D</i> )+N <sub>2</sub> O <sup>a</sup>	2315.1 ( $\sigma^+$ ) [2282.1 ( $\sigma^+$ )]	1317.6 ( $\sigma^+$ ) [1298.3 ( $\sigma^+$ )]	593.0 ( $\pi$ ) [596.3 ( $\pi$ )]				6.9
NO+NO <sup>b</sup>	1915.1 ( $\sigma^+$ ) [1904.2 ( $\sigma^+$ )]						5.5
N <sub>2</sub> +O <sub>2</sub> ( <i>a</i> <sup>1</sup> $\Delta_g$ ) <sup>b</sup>	2365.9 ( $\sigma_g^+$ )(N <sub>2</sub> ) [2358.6 ( $\sigma_g^+$ )]	1450.0 ( $\sigma_g^+$ )(O <sub>2</sub> ) [1483.5 ( $\sigma_g^+$ )]					5.4
Reaction (1)							
MIN A1	2280.9 ( <i>a</i> ')	1300.2 ( <i>a</i> ')	612.9 ( <i>a</i> ')	603.2 ( <i>a</i> '')	37.7 ( <i>a</i> ')	26.2 ( <i>a</i> ')	6.9
TS A1	423.0 <i>i</i> ( <i>a</i> ')	2241.4 ( <i>a</i> ')	1304.9 ( <i>a</i> ')	640.0 ( <i>a</i> '')	629.6 ( <i>a</i> ')	76.6( <i>a</i> ')	7.0
MIN B1	1672.4 ( <i>a</i> <sub>g</sub> )	1520.2 ( <i>b</i> <sub>u</sub> )	810.2 ( <i>a</i> <sub>g</sub> )	496.6 ( <i>a</i> <sub>g</sub> )	401.8 ( <i>b</i> <sub>u</sub> )	245.3 ( <i>a</i> <sub>u</sub> ) <sup>c</sup>	7.3
TS B1	561.4 <i>i</i> ( <i>a</i> <sub>g</sub> )	1610.5 ( <i>a</i> <sub>g</sub> )	1604.7 ( <i>b</i> <sub>u</sub> )	611.1 ( <i>a</i> <sub>g</sub> )	398.4 ( <i>b</i> <sub>u</sub> )	157.7 ( <i>a</i> <sub>u</sub> ) <sup>c</sup>	6.3
MIN C1	1889.9 ( <i>a</i> <sub>g</sub> ) [1861.1 ( <i>a</i> <sub>g</sub> )] <sup>d</sup>	1889.7 ( <i>b</i> <sub>u</sub> ) [1747.1 ( <i>b</i> <sub>u</sub> )] <sup>e</sup>	61.2 ( <i>a</i> <sub>g</sub> )	40.5 ( <i>a</i> <sub>u</sub> )	27.6 ( <i>a</i> <sub>g</sub> )	24.6 ( <i>b</i> <sub>u</sub> )	5.6
TS C1	19.9 <i>i</i> ( <i>a</i> )	1890.3 ( <i>a</i> )	1889.4 ( <i>b</i> )	51.6 ( <i>a</i> )	39.5 ( <i>b</i> )	22.7 ( <i>a</i> )	5.6
MIN D1 <sup>c</sup>	1890.5 ( <i>a</i> <sub>1</sub> ) [1863.4 ( <i>a</i> <sub>1</sub> )]	1886.2 ( <i>b</i> <sub>1</sub> ) [1776.3 ( <i>b</i> <sub>1</sub> )]	113.2 ( <i>b</i> <sub>1</sub> ) [242.9 ( <i>b</i> <sub>1</sub> )]	85.0 ( <i>a</i> <sub>1</sub> ) [299.3 ( <i>a</i> <sub>1</sub> )]	41.0 ( <i>a</i> <sub>2</sub> ) [103.4 ( <i>a</i> <sub>2</sub> )]	31.2 ( <i>a</i> <sub>1</sub> ) [175.4 ( <i>a</i> <sub>1</sub> )]	5.8 [6.4]
TS E1 <sup>f</sup>	1277.7 <i>i</i> ( <i>a</i> )	217.2 <i>i</i> ( <i>a</i> )	1222.0 ( <i>a</i> )	928.3 ( <i>a</i> )			5.2
MIN E1	1485.8 ( <i>a</i> <sub>1</sub> )	1116.3 ( <i>b</i> <sub>1</sub> )	1072.8 ( <i>a</i> <sub>1</sub> )	805.2 ( <i>b</i> <sub>1</sub> )	792.1 ( <i>a</i> <sub>1</sub> )	677.4 ( <i>a</i> <sub>2</sub> )	8.5
TS F1	3034.4 <i>i</i> ( <i>a</i> )	1227.3 ( <i>a</i> )	877.2 ( <i>b</i> )	754.3 ( <i>a</i> )	491.7 ( <i>b</i> )	107.6 ( <i>a</i> )	4.9
Reaction (2)							
MIN A2	2272.7 ( <i>a</i> ')	1296.1 ( <i>a</i> ')	603.6 ( <i>a</i> '')	603.0 ( <i>a</i> ')	65.0 ( <i>a</i> ')	48.7 ( <i>a</i> ')	7.0
TS A2	553.1 <i>i</i> ( <i>a</i> ')	2247.2 ( <i>a</i> ')	1197.6 ( <i>a</i> ')	605.3 ( <i>a</i> ')	575.5 ( <i>a</i> '')	164.5 ( <i>a</i> ')	6.8
MIN B2	2272.4 ( <i>a</i> ')	1125.7 ( <i>a</i> ')	629.5 ( <i>a</i> ')	545.1 ( <i>a</i> '')	507.8 ( <i>a</i> ')	223.1 ( <i>a</i> ')	7.6
TS B2	1098.7 <i>i</i> ( <i>a</i> ')	2160.4 ( <i>a</i> ')	841.4 ( <i>a</i> ')	633.8 ( <i>a</i> ')	278.5 ( <i>a</i> '')	195.9 ( <i>a</i> ')	5.9
Reactions (1)–(2) connection							
TS A3	622.3 <i>i</i> ( <i>a</i> )	1585.9 ( <i>a</i> )	798.2 ( <i>a</i> )	630.1 ( <i>a</i> )	551.1 ( <i>a</i> )	438.3 ( <i>a</i> )	5.8

<sup>a</sup>Experimental data taken from Ref. 57.

<sup>b</sup>Experimental data taken from Ref. 55.

<sup>c</sup>Frequencies calculated numerically by fitting small out-of-plane distortions to a quadratic polynomial.

<sup>d</sup>Experimental data taken from Ref. 32.

<sup>e</sup>Experimental data taken from Ref. 31.

<sup>f</sup>Only four symmetry-adapted ( $C_2$ ) frequencies could be calculated, two of which are imaginary (see the text). In addition to the two positive frequencies, the third, fifth, and sixth frequencies of TS *F1* have been assumed to calculate the ZPE.

When the ON distance decreases, the weight of the first configuration diminishes and that of the second one augments, finally reaching MIN *B1*. The change in importance for configurations  $13 a'^2 2 a''^2$  and  $12 a'^2 3 a''^2$  can be attributed to the gradual shifting of the O(<sup>1</sup>*D*)  $2p_x$  electron (*a*') towards the  $2p_z$  orbital (*a*''), both being initially singly occupied, with simultaneous formation of the ON bond. In fact, this process can be seen as an attack of N<sub>2</sub>O to O(<sup>1</sup>*D*), in which the two electrons situated in an in-plane  $\pi$  N<sub>2</sub>O orbital displace the O(<sup>1</sup>*D*)  $2p_x$  electron to the  $2p_z$  orbital, thus forming a dative ON bond. In this way the system gains one new bonding at the cost of only an electronic recoupling, and no bond breakage takes place. This would allow one to understand the absence of an energy barrier (including the ZPE) for reaction (1). From MIN *B1* to TS *B1* the configuration  $12 a'^2 3 a''^2$  loses its importance and somewhere between TS *B1* and MIN *C1* the leading configuration changes, as can be seen in  $C_{2h}$  symmetry. A double excitation from an  $a_u$  orbital ( $\pi$  NN bonding) to an  $a_g$  one ( $\sigma$  NN bonding) has occurred. Thus, the double NN bonding breaks and some  $\sigma$  electronic density passes from the NO bonds to the NN bond. Nearer to products the NN bond acquires increasingly diradical character, as indicated by the almost equal weight of the

two leading configurations related (in  $C_{2h}$  symmetry) by the double excitation from an  $a_g$  ( $\sigma$  NN bonding) to a  $b_u$  ( $\sigma$  NN antibonding) orbital. These orbitals are the “+” and “−” combinations of the  $\pi^*$  orbitals of each NO fragment, which are equally occupied at an infinite distance.

In the alternative *cis*-MERP of reaction (1) (Fig. 1), a new electronic configuration is predominant in TS *E1*, MIN *E1*, and TS *F1*. MIN *E1* could be compared with MIN *B1* because both stationary points are of an essentially closed-shell nature, the main difference being the OO single bond in the former. In TS *E1* an out-of-plane rotation of one NO moiety with respect to the other takes place, allowing for the *cis*–*trans* isomerization between MIN *E1* and MIN *B1*. MIN *E1* can also evolve through TS *F1* keeping  $C_{2v}$  symmetry while the NO fragments separate from each other on their way to products.

For reaction (2), as it can be seen from its MERP in Fig. 2, the attack of the O(<sup>1</sup>*D*) atom to the other end of the N<sub>2</sub>O molecule leads at the CASSCF level to a very different behavior from that observed in reaction (1). Thus, the system now passes through two minima [MIN *A2* (vdW) and MIN *B2*] and two TSs (TS *A2* and TS *B2*) of  $C_s$  symmetry (<sup>1</sup>*A'*), with little distortion of the N<sub>2</sub>O fragment (i.e., they

TABLE IV. Energies of the stationary points calculated at different levels. Energies are given in kcal mol<sup>-1</sup> with respect to reactants. For MIN C1, TS C1, and MIN D1, it is more convenient to give them relative to products. Energies with (without) ZPE without (in) parentheses.

Stationary point	CASSCF(14,12)	CASPT2//CASSCF(14,12)	CASSCF(18,14)	CASPT2//CASSCF(18,14)	Experiment <sup>a</sup>
O( <sup>1</sup> D)+N <sub>2</sub> O	0.0(0.0)	0.0(0.0)	0.0(0.0)	0.0(0.0)	0.0(0.0)
NO+NO	-77.5(-76.1)	-81.3(-79.9)	-79.7(-78.3)	-81.9(-80.5)	-81.8(-80.4)
N <sub>2</sub> +O <sub>2</sub> ( <sup>a</sup> 1Δ <sub>g</sub> )	-102.3(-100.8)	-105.3(-103.9)	-102.8(-101.3)	-105.0(-103.5)	-102.1(-100.9)
Reaction (1)					
MIN A1	-0.2(-0.2)	-0.5(-0.5)	-0.2(-0.2)	-0.6(-0.6)	
TS A1	12.5(12.4)	-7.2(-7.3)	5.8(5.7)	-5.1(-5.2)	
MIN B1 <sup>b</sup>			-41.1(-41.5)	-65.8(-66.2)	
TS B1 <sup>b</sup>			-40.5(-39.9)	-62.2(-61.6)	
MIN C1	-0.1(-0.2)	-0.7(-0.8)	-0.1(-0.2)	-0.7(-0.8)	-2.1(-3.1) <sup>c</sup>
TS C1	-0.1(-0.2)	-0.8(-0.9)	0.0(-0.1)	-0.7(-0.8)	
MIN D1	0.0(-0.3)	-1.3(-1.6)	0.0(-0.3)	-1.7(-2.0)	
TS E1 <sup>b</sup>			-1.3(0.4)	-25.3(-23.6)	
MIN E1	-12.3(-13.9)	-35.8(-37.4)	-16.6(-18.2)	-36.9(-38.5)	
TS F1	7.6(9.6)	-20.7(-18.7)	-2.6(-0.6)	-26.0(-24.0)	
Reaction (2)					
MIN A2	-0.5(-0.6)	-1.0(-1.1)	-0.5(-0.6)	-1.0(-1.1)	
TS A2	7.9(8.0)	-5.1(-5.0)	6.2(6.3)	-4.6(-4.5)	
MIN B2	0.3(-0.4)	-8.3(-9.0)	-1.7(-2.4)	-9.1(-9.8)	
TS B2	4.9(5.9)	-9.2(-10.0)	2.1(3.1)	-11.9(-10.9)	
Reactions (1)-(2) connection					
TS A3	14.6(15.8)	-6.8(-5.6)			

<sup>a</sup>Experimental data derived from Refs. 54–57.<sup>b</sup>These stationary points were not found at the (14,12) level (see Table III).<sup>c</sup>Derived from experimental values of *D*<sub>0</sub> and ZPE summarized in Ref. 25.

TABLE V. Electronic configurations and active spaces of the stationary points at the CASSCF(18,14) level.

	Inactive	Active	Electronic configurations <sup>a</sup>
Reaction (1)			
O+N <sub>2</sub> O ( <i>C<sub>s</sub></i> )	6 <i>a</i> '	10 <i>a</i> ' + 4 <i>a</i> "	13 <i>a</i> ' <sup>2</sup> 2 <i>a</i> " <sup>2</sup> /12 <i>a</i> ' <sup>2</sup> 3 <i>a</i> " <sup>2</sup> (-0.67/0.67)
MIN A1 ( <i>C<sub>s</sub></i> )	"	"	(-0.66/0.67)
TS A1 ( <i>C<sub>s</sub></i> )	"	"	(-0.32/0.88)
MIN B1 ( <i>C<sub>2h</sub></i> )	3 <i>a<sub>g</sub></i> + 3 <i>b<sub>u</sub></i> (6 <i>a</i> ')	5 <i>a<sub>g</sub></i> + 2 <i>a<sub>u</sub></i> + 2 <i>b<sub>g</sub></i> + 5 <i>b<sub>u</sub></i> (10 <i>a</i> ' + 4 <i>a</i> "	6 <i>a<sub>g</sub></i> <sup>2</sup> 2 <i>a<sub>u</sub></i> <sup>2</sup> 1 <i>b<sub>g</sub></i> <sup>2</sup> 6 <i>b<sub>u</sub></i> <sup>2</sup> (12 <i>a</i> '3 <i>a</i> "(0.89)
TS B1 ( <i>C<sub>2h</sub></i> )	"	"	(0.88)
MIN C1 ( <i>C<sub>2h</sub></i> )	"	"	7 <i>a<sub>g</sub></i> <sup>2</sup> 1 <i>a<sub>u</sub></i> <sup>2</sup> 1 <i>b<sub>g</sub></i> <sup>2</sup> 6 <i>b<sub>u</sub></i> <sup>2</sup> /6 <i>a<sub>g</sub></i> <sup>2</sup> 1 <i>a<sub>u</sub></i> <sup>2</sup> 1 <i>b<sub>g</sub></i> <sup>2</sup> 7 <i>b<sub>u</sub></i> <sup>2</sup> (13 <i>a</i> '2 <i>a</i> "(0.69/-0.63)
TS C1 ( <i>C<sub>2</sub></i> )	3 <i>a</i> + 3 <i>b</i>	7 <i>a</i> + 7 <i>b</i>	8 <i>a</i> <sup>2</sup> 7 <i>b</i> <sup>2</sup> /7 <i>a</i> <sup>2</sup> 8 <i>b</i> <sup>2</sup> (0.85/-0.37)
MIN D1 ( <i>C<sub>2v</sub></i> )	3 <i>a</i> <sub>1</sub> + 3 <i>b</i> <sub>2</sub> (6 <i>a</i> ')	5 <i>a</i> <sub>1</sub> + 2 <i>a</i> <sub>2</sub> + 2 <i>b</i> <sub>1</sub> + 5 <i>b</i> <sub>2</sub> (10 <i>a</i> ' + 4 <i>a</i> "	7 <i>a</i> <sub>1</sub> <sup>2</sup> 1 <i>a</i> <sub>2</sub> <sup>2</sup> 1 <i>b</i> <sub>1</sub> <sup>2</sup> 6 <i>b</i> <sub>2</sub> <sup>2</sup> /6 <i>a</i> <sub>1</sub> <sup>2</sup> 1 <i>a</i> <sub>2</sub> <sup>2</sup> 1 <i>b</i> <sub>1</sub> <sup>2</sup> 7 <i>b</i> <sub>2</sub> <sup>2</sup> (13 <i>a</i> '2 <i>a</i> "(0.72/-0.60)
TS E1 ( <i>C<sub>2</sub></i> )	3 <i>a</i> + 3 <i>b</i>	7 <i>a</i> + 7 <i>b</i>	8 <i>a</i> <sup>2</sup> 7 <i>b</i> <sup>2</sup> /7 <i>a</i> <sup>2</sup> 8 <i>b</i> <sup>2</sup> (0.81/-0.45)
MIN E1 ( <i>C<sub>2v</sub></i> )	3 <i>a</i> <sub>1</sub> + 3 <i>b</i> <sub>2</sub> (6 <i>a</i> ')	5 <i>a</i> <sub>1</sub> + 2 <i>a</i> <sub>2</sub> + 2 <i>b</i> <sub>1</sub> + 5 <i>b</i> <sub>2</sub> (10 <i>a</i> ' + 4 <i>a</i> "	7 <i>a</i> <sub>1</sub> <sup>2</sup> 1 <i>a</i> <sub>2</sub> <sup>2</sup> 2 <i>b</i> <sub>1</sub> <sup>2</sup> 5 <i>b</i> <sub>2</sub> <sup>2</sup> /6 <i>a</i> <sub>1</sub> <sup>2</sup> 1 <i>a</i> <sub>2</sub> <sup>2</sup> 2 <i>b</i> <sub>1</sub> <sup>2</sup> 6 <i>b</i> <sub>2</sub> <sup>2</sup> (12 <i>a</i> '3 <i>a</i> "(0.92/0.17)
TS F1 ( <i>C<sub>2v</sub></i> )	"	"	(0.78/-0.51)
2 NO ( <i>C<sub>2v</sub></i> )	"	"	7 <i>a</i> <sub>1</sub> <sup>2</sup> 1 <i>a</i> <sub>2</sub> <sup>2</sup> 1 <i>b</i> <sub>1</sub> <sup>2</sup> 6 <i>b</i> <sub>2</sub> <sup>2</sup> /6 <i>a</i> <sub>1</sub> <sup>2</sup> 1 <i>a</i> <sub>2</sub> <sup>2</sup> 1 <i>b</i> <sub>1</sub> <sup>2</sup> 7 <i>b</i> <sub>2</sub> <sup>2</sup> (13 <i>a</i> '2 <i>a</i> "(-0.66/0.66)
Reaction (2)			
O+N <sub>2</sub> O ( <i>C<sub>s</sub></i> )	6 <i>a</i> '	10 <i>a</i> ' + 4 <i>a</i> "	13 <i>a</i> ' <sup>2</sup> 2 <i>a</i> " <sup>2</sup> /12 <i>a</i> ' <sup>2</sup> 3 <i>a</i> " <sup>2</sup> (-0.67/0.67)
MIN A2 ( <i>C<sub>s</sub></i> )	"	"	(-0.66/0.67)
TS A2 ( <i>C<sub>s</sub></i> )	"	"	(-0.30/0.89)
MIN B2 ( <i>C<sub>s</sub></i> )	5 <i>a</i> ' + 1 <i>a</i> "	11 <i>a</i> ' + 3 <i>a</i> "	12 <i>a</i> ' <sup>2</sup> 3 <i>a</i> " <sup>2</sup> (0.94)
TS B2 ( <i>C<sub>s</sub></i> )	"	"	(0.92)
N <sub>2</sub> +O <sub>2</sub> ( <sup>a</sup> 1Δ <sub>g</sub> ) ( <i>C<sub>2v</sub></i> )	6 <i>a</i> <sub>1</sub> (6 <i>a</i> ')	6 <i>a</i> <sub>1</sub> + 4 <i>b</i> <sub>1</sub> + 4 <i>b</i> <sub>2</sub> (10 <i>a</i> ' + 4 <i>a</i> "	10 <i>a</i> <sub>1</sub> <sup>2</sup> 2 <i>b</i> <sub>1</sub> <sup>2</sup> 3 <i>b</i> <sub>2</sub> <sup>2</sup> /10 <i>a</i> <sub>1</sub> <sup>2</sup> 3 <i>b</i> <sub>1</sub> <sup>2</sup> 2 <i>b</i> <sub>2</sub> <sup>2</sup> (12 <i>a</i> ' <sup>2</sup> 3 <i>a</i> " <sup>2</sup> /13 <i>a</i> ' <sup>2</sup> 2 <i>a</i> " <sup>2</sup> )(0.65/-0.65)
Reactions (1)-(2) connection			
TS A3 ( <i>C<sub>1</sub></i> )	6 <i>a</i>	14 <i>a</i>	15 <i>a</i> <sup>2</sup> (0.81/-0.43) <sup>b</sup>

<sup>a</sup>Leading configurations and CI coefficients for each stationary point are given. For the configurations, the number of orbitals belonging to each irreducible representation is indicated.<sup>b</sup>Results obtained at the CASSCF(14,12) level. The two different main electronic configurations cannot be distinguished by symmetry (the stationary point has *C*<sub>1</sub> symmetry).

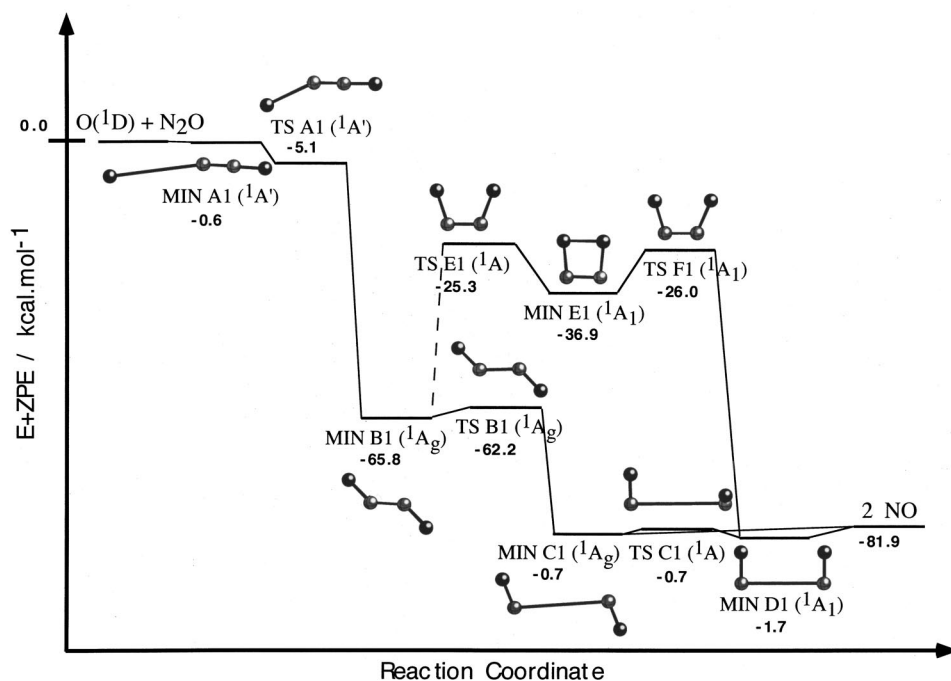


FIG. 1. Schematic representation of the stationary points [CASSCF(18,14)] and energy profile [CASPT2//CASSCF(18,14) energy plus CASSCF(14,12) ZPE] for reaction (1). Energies are given relative to reactants, O(<sup>1</sup>D) + N<sub>2</sub>O, except for MIN C1, TS C1, and MIN D1, whose energies are given relative to products, 2 NO.

are placed in the entrance zone). From the TS with the shorter OO distance (TS B2) the energy goes down abruptly, bringing about the products. In summary, for this MERP we have the following: O(<sup>1</sup>D) + N<sub>2</sub>O → MIN A2 → TS A2 → MIN B2 → TS B2 → N<sub>2</sub> + O<sub>2</sub>(*a*<sup>1</sup>Δ<sub>g</sub>).

The marked reactant-like diradical character of MIN A2 and TS A2 becomes clear from Table V, which changes into an essentially closed-shell situation in MIN B2 and TS B2. The formation of the OO bond takes place in a way analogous to reaction (1) up to TS A2, thus implying also that reaction (2) is not likely to have an energy barrier, as observed in the calculations and consistently with experimental

data. From TS B2, and as the ON bond elongates, another configuration becomes increasingly important, representing the redistribution of the electronic density to reach a pure diradical character in products [one electron placed in each π<sub>g</sub><sup>\*</sup> orbital of O<sub>2</sub>(*a*<sup>1</sup>Δ<sub>g</sub>)].

As concerns the quality of the active spaces selected, in Table II we note the important qualitative differences that exist between the CASSCF (14,12) and (18,14) results in reaction (1), whereas both levels of calculation provide a very similar description of reaction (2). For reaction (1) three stationary points which are present at the CASSCF(18,14) level (MIN B1, TS B1, and TS E1) are absent at the

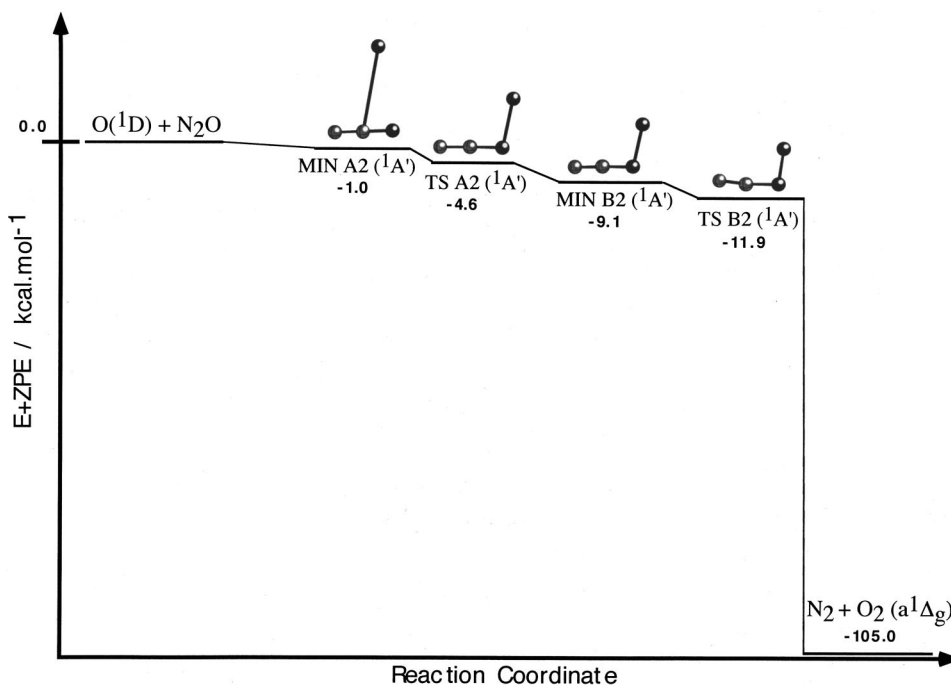


FIG. 2. Schematic representation of the stationary points [CASSCF(18,14)] and energy profile [CASPT2//CASSCF(18,14) energy plus CASSCF(14,12) ZPE] for reaction (2). Energies are given relative to reactants, O(<sup>1</sup>D) + N<sub>2</sub>O.

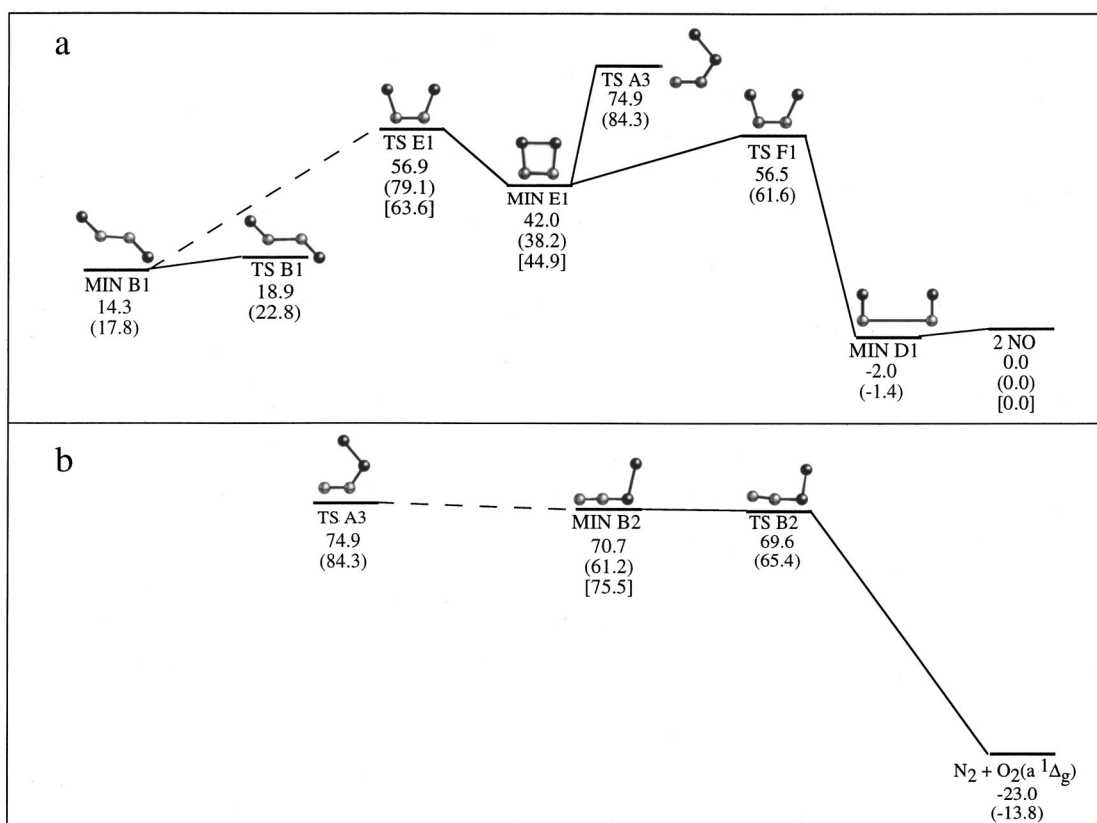


FIG. 3. Sketch of the energies of the stationary points (in kcal mol<sup>-1</sup>) on the <sup>1</sup>A' PES relative to products, 2 NO, for (a) reaction (1) and (b) reaction (2). The vertical scale is approximate and reflects the energies (without ZPE) of the structures reported in Figs. 1 and 2. The nomenclature of those structures is also kept. The energy data correspond to the following levels: CASPT2 //CASSCF(18,14)/6-311G(2d) except for TS A3 (CASPT2//CASSCF(14,12)/6-311G(2d)) (present work, plain text); BD(T)/aug-cc-pVTZ (Ref. 17, in parentheses); CASPT2//CASSCF(14,12)/6-311+G(2d) for MIN E1, TS E1/F1; CASPT2(10,10)/6-311+G(2d)//CASSCF(10,10)/6-31G(d) for MIN B2 (Refs. 35 and 37, in brackets). Note that two connections, namely, those between TS E1 and MIN B1 [reaction (1)] and between TS A3 and MIN B2 [reaction (2)] could not be rigorously established, as indicated with dashed lines. Note also that only one connection for TS A3 has been indicated in subfigures (a) and (b).

CASSCF(14,12) level. In addition, one transition state (TS F1) changes its symmetry from C<sub>2</sub> (nonplanar structure) to C<sub>2v</sub> (planar structure). However, we believe that TS F1 at the CASSCF(14,12) level is the equivalent of TS E1 at the CASSCF(18,14) one, but in the former case TS F1 connects with the *cis*-(NO)<sub>2</sub> dimer near products, because MIN B1 does not exist at the CASSCF(14,12) level. The entrance and exit zones of reaction (1) are described in a similar manner with both active spaces (the same structures are obtained with slightly varying geometries). The discrepancies in the intermediate zone of this reaction are due to the two relevant 2s active orbitals mainly centered in the N atoms lacking in the (1,4,12) space. Their importance can be estimated by their NOONs in this zone, whose values are (1.9883, 1.9759) in MIN B1, (1.9893, 1.9785) in TS B1, (1.9920, 1.9794) in TS E1, and (1.9915, 1.9819) in TS F1. This reinforces the criterion explained above based on the NOONs, because at least one of the orbitals has an occupancy near 1.98, while for the other stationary points of reactions (1) and (2) the associated NOONs are always larger. The role of the 2s orbitals must be to strengthen the NN bonding, thus making feasible the existence of MIN B1 and TS B1, and the connection of MIN E1 and MIN B1 through the nonplanar TS E1, though the latter could not be fully checked.

## B. Comparison with previous *ab initio* and DFT results

At this point it is interesting to compare with other results from the literature obtained with different theoretical methods. In Fig. 3 the structures obtained in the present work that were also studied in previous works are schematized. We already commented in Sec. I that there is a wealth of theoretical studies on the exit zone shallow (NO)<sub>2</sub> minima of reaction (1) and the TS connecting them. For a more detailed discussion of this region see Ref. 25.

As concerns reaction (1), in the *trans*-MERP a structure corresponding to MIN B1 has been characterized at the second-order Møller–Plesset (MP2) level,<sup>16</sup> but its stability with respect to reactants [−95.9 kcal mol<sup>-1</sup> (UMP2)] is quite different from that found in the present study [Fig. 3(a)]. Also, in reaction (1) structures analogous to MIN E1 and TS E1 have been reported in the context of studies on high-energy isomers. Thus, calculations at the MP2<sup>35</sup> and CASPT2//CASSCF<sup>35,37</sup> levels are available in the literature. In Ref. 37, which is the more directly comparable to the present study, (10,10) and (14,12) active spaces were used with several Pople basis sets. The geometries of MIN E1 obtained with these two active spaces are very similar to each other and to the results given here, whereas there is a

significant difference in the structure of TS *E1* (Table II). Thus, it is reported as pertaining to the  $C_1$  symmetry group at the CASSCF(10,10) and (14,12) levels, but our results indicate that the CASSCF(18,14) structure has  $C_2$  symmetry. The relative energies can be compared to those obtained in the present work [Fig. 3(a)]. Note the change in the TS *E1* energy barrier with respect to the one derived from Ref. 37, the latter being larger by about 6 kcal mol<sup>-1</sup>. This indicates again the importance of the additional 2s-type MOs in the (18,14) active space with respect to the (14,12) one.

For reaction (2) one of the stationary points (MIN *B2*) has been noted previously also as a high-energy isomer.<sup>33-35</sup> Its characterization was carried out at the CASSCF(10,10), CISD (configuration interaction with single and double excitations) and MRCI (multireference configuration interaction) levels. There is a good general accord both in the geometries reported for MIN *B2* and our own, and in its energy relative to 2 NO [Fig. 3(b)]. The shortening of the OO distance from CASSCF when going to CISD and MRCI methods, that introduce dynamical correlation, is remarkable.

We should mention that other high-energy structures were characterized on the ground PES,<sup>33-38</sup> but connections with the rest of stationary points and with reactants were not reported. Thus, they are possibly not relevant to the present study in which we have focused on the reactivity of O(<sup>1</sup>*D*) + N<sub>2</sub>O.

Most of the structures reported in the present work, and high-energy structures obtained in previous works, were obtained recently at the *ab initio* BD(T) (Brueckner doubles approach with perturbative triplets) and DFT (B3LYP) levels of theory.<sup>17</sup> In reaction (1), structures corresponding to MIN *B1* and TS *C1* in the *trans*-MERP and to TS *E1*, MIN *E1*, TS *F1*, and MIN *D1* in the *cis*-one were found [Fig. 3(a)]. Also, in reaction (2) stationary points analogous to MIN *B2* and TS *B2* were located [Fig. 3(b)]. Besides, a TS between reactions (1) and (2) was noted, connecting MIN *E1* with MIN *B2*. We have also obtained this structure, which is labeled TS *A3* in Table II and Fig. 3. However, the van der Waals minima and TSs on the entrance zone of both reactions and the isomeric structures to the vdW *cis*-dimer (MIN *D1*) presented here were not located previously.

As commented on above, we also performed a study of the ground <sup>1</sup>*A'* PES at the DFT level with several functionals and basis sets.<sup>18</sup> The best results were obtained at the B3LYP/6-311G(2*d*) level, although only a moderately good representation of reactants and products was reached. This is particularly true for the diradical species, O(<sup>1</sup>*D*) and O<sub>2</sub>(<sup>1</sup> $\Delta_g$ ), which are affected by the spin contamination problem. Even when projection of the wave function to eliminate the triplet contribution was performed, the method we used<sup>42</sup> did not seem to yield results of enough quality. With this method we obtained stationary points analogous to those reported in Figs. 1 and 2. Among the structures obtained in our work, those that were also characterized in Ref. 17 show very similar geometries and frequencies. However, we found a certain spin contamination in TS *B1* and in the vdW (NO)<sub>2</sub> dimers. In particular, TS *B1* presents  $C_{2h}$  symmetry, whereas it is found to have  $C_2$  symmetry in Ref. 17. From this comparison one can conclude that a good overall

agreement between comparable structures was achieved.

On the other hand, there are remarkable differences between the results in Ref. 17 and those presented in this work at the CASPT2//CASSCF level. Thus, in Ref. 17 the B3LYP and BD(T) wave functions are based on a single determinant, and it is doubtful that the electronic correlation introduced by these methods could correct for the lacking diradical character when necessary. The alternative of using an unrestricted approach has the spin contamination problem as an important limitation, as explained above. In particular, note the unsatisfactory geometry and frequencies of the pure diradical O<sub>2</sub>(<sup>1</sup> $\Delta_g$ ) obtained at the unrestricted B3LYP level, as pointed out by the authors themselves. The incorrectness of the wave function is also reflected in the energy difference between 2 NO and N<sub>2</sub>+O<sub>2</sub>(<sup>1</sup> $\Delta_g$ ), about 6 kcal mol<sup>-1</sup> deviating from experiment at the restricted BD(T)/aug-cc-pVTZ level. Note also that for the *cis*-(NO)<sub>2</sub> dimer distances shorter than the experiment are always obtained with either B3LYP or BD(T). In previous DFT works, including our calculations, the same tendency was found.<sup>18,26,27</sup> The geometries and relative energies (Fig. 3) of the rest of the minima common to Ref. 17 and this work are rather similar, as could be expected from their marked closed-shell character.

The transition states are also a particularly difficult case, because a mixing of configurations is commonly found for this kind of structure. First, note the much higher barriers for the interconversion of MIN *E1* and MIN *B1* (i.e., through TS *E1*) and for the passage from MIN *E1* to products (TS *F1*) obtained at the BD(T)/aug-cc-pVTZ level when compared to the CASPT2 ones [Fig. 3(a)], particularly for the former. However, the TS *B1* barrier relative to MIN *B1* is very similar at both levels, as could be expected by the essentially closed-shell character of these stationary points (see Table V). There are also interesting differences in the symmetry of TS *E1*, TS *F1*, and TS *B1*, as these structures belong to the  $C_2$ ,  $C_{2v}$ , and  $C_{2h}$  point groups at the CASSCF(18,14) level but to  $C_{2v}$ ,  $C_2$ , and  $C_2$  according to Ref. 17, respectively. We were also able to characterize the TS linking reactions (1) and (2), labeled TS *A3*, at the CASSCF(14,12) level, obtaining the results reported in Table II. The main electronic configurations of this TS (Table V) suggest a strong diradical character, which would not be correctly treated at the B3LYP or BD(T) levels. For instance, note the energy difference of about 10 kcal mol<sup>-1</sup> reported in Fig. 3 between the CASPT2//CASSCF and BD(T) results. The ON distance of TS *A3* is about 0.15 Å longer at the CASSCF level than that obtained at the B3LYP level, the rest of the parameters being rather similar. It is worth mentioning that broken-symmetry problems were detected for the CASSCF wave function. They were also detected in previous work of our own.<sup>25</sup> It is likely that this structure is not correctly treated either at the B3LYP, BD(T), or CASSCF levels.

Finally, in a recent work,<sup>19</sup> restricted scans over the ground and excited <sup>1</sup>*A'* and <sup>1</sup>*A''* PESs of the system were performed at the CASPT2//CASSCF level of theory, using a (10,8) active space for reaction (1) and a (10,10) one for reaction (2), and employing a basis set of double-zeta quality. In particular, potential energy curves with respect to the O(<sup>1</sup>*D*)-N distance with a fixed O(<sup>1</sup>*D*)-N-N angle were

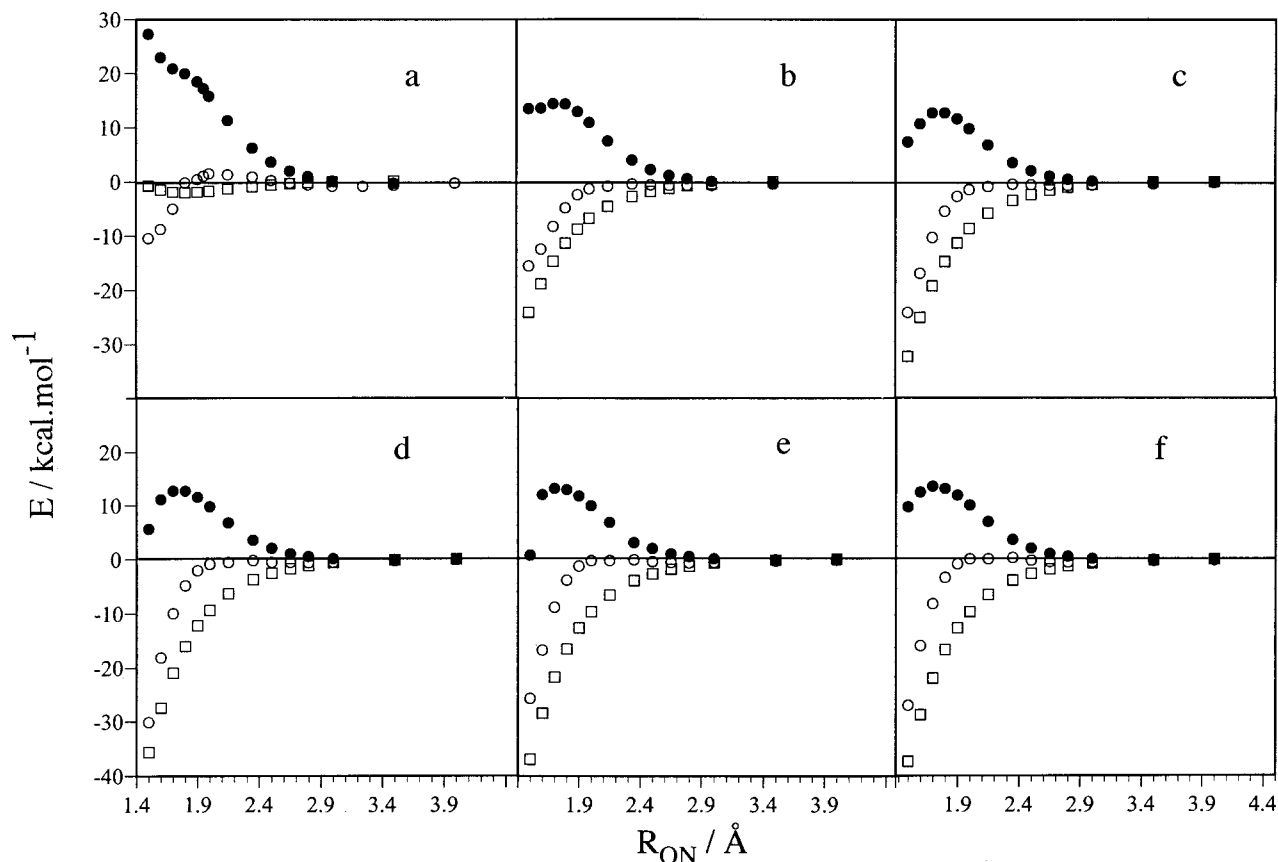


FIG. 4. Energy relative to reactants, O(<sup>1</sup>D)+N<sub>2</sub>O, in front of the ON attack distance for reaction (1) at different ONN angles of approach, with the N<sub>2</sub>O geometry kept fixed at its equilibrium CASSCF(14,12) value: (a) 80°; (b) 100°; (c) 120°; (d) 140°; (e) 160°; (f) 180°. Symbols correspond to the following type of calculation: CASPT2 (○), CASSCF (●), and LEPS empirical surface (□). See the text.

constructed, assuming the equilibrium geometry for the N<sub>2</sub>O molecule. The authors observe the same trends as found in the present work, i.e., the CASSCF curves present a considerable entrance barrier, whereas the CASPT2 ones are very flat, bearing a small barrier at an O(<sup>1</sup>D)–N distance rather shifted from the CASSCF value.

From a reduced-dimensionality study of the ground <sup>1</sup>A' PES,<sup>19</sup> in which grids of points at several fixed values of the O(<sup>1</sup>D)–N–N angle were calculated with respect to only two degrees of freedom, i.e., the O(<sup>1</sup>D)–N and N–N distances, the authors discuss qualitatively the rovibrational distribution for the products of reaction (1), 2 NO. They attach great importance to a very deep collinear minimum (about 50 kcal mol<sup>-1</sup> below reactants) and to its exit barrier to products (some 20 kcal mol<sup>-1</sup> above reactants), as well as to the ever-decreasing character of the PES for O(<sup>1</sup>D)–N–N angles far from collinearity. These features of the PES would lead to two very different reactive mechanisms, which can be described as complex and direct, respectively. Their study of reaction (2) is more limited and we will not refer to it in the following.

There are important differences between the work reported in Ref. 19 and our own. First, we believe that a discussion of the dynamics of reaction (1) in terms of a partial, three-dimensional study of the six-dimensional O(<sup>1</sup>D) + N<sub>2</sub>O system is not quite justified, as it may lead to misleading conclusions. The presence of a deep minimum and a

high barrier for collinear geometries must be a consequence of the study being partial. If one takes a look at Fig. 1 in this work, it is clear that a huge distortion of the NNO moiety is required for the system to reach a minimum, e.g., MIN B1. Even though MIN B1 is placed about 65 kcal mol<sup>-1</sup> below reactants, its barrier to products is not larger than 3–4 kcal mol<sup>-1</sup> (i.e., through TS B1). On the other hand, the wide entrance angle and the energy decreasing character of the PES for angles far from collinearity are in qualitative agreement with our own results. A second comment concerns the size of the active spaces used. In our opinion, those used in Ref. 19, i.e., a (10,8) active space for reaction (1) and a (10,10) one for reaction (2), are not large enough to yield quantitative results. In fact, they must lack some important orbitals, given that a minimum CASSCF active space comprises 18 electrons in 14 orbitals. One could argue that CASPT2 could correct for it by adding all the electronic correlation not considered at the CASSCF level. However, some problems such as a low and nonhomogeneous reference weight in the CASPT2 wave function and/or the appearance of intruder states may be present [i.e., it must be corrected for even in the (14,12) case, see below]. Therefore, we conclude that a full-dimensional study of the system with a more extensive active space than those employed in Ref. 19 is needed if a reliable PES useful in dynamics studies is to be obtained.

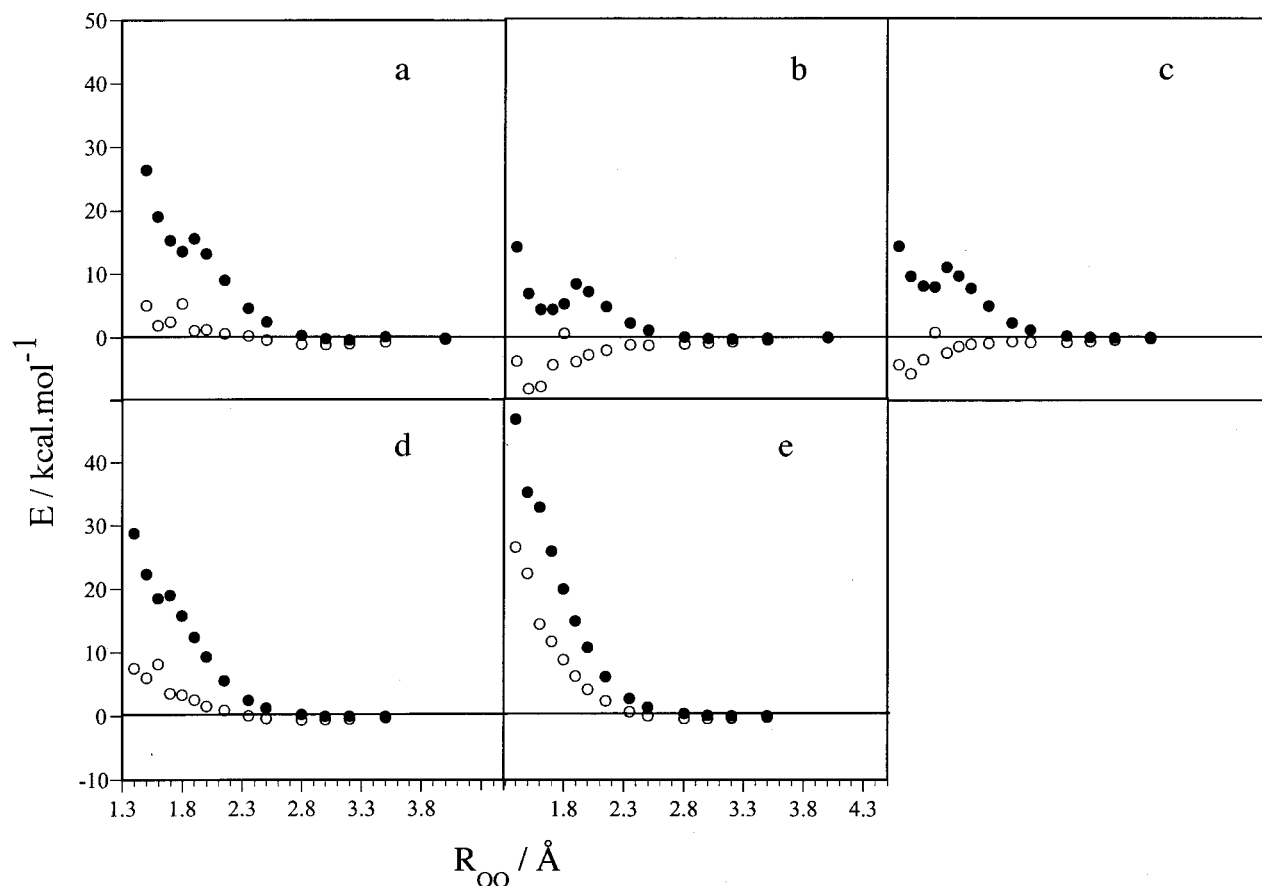


FIG. 5. Energy relative to reactants,  $O(^1D)+N_2O$ , in front of the OO attack distance for reaction (2) at different OON angles of approach, with the  $N_2O$  geometry kept fixed at its equilibrium CASSCF(14,12) value: (a)  $80^\circ$ ; (b)  $100^\circ$ ; (c)  $120^\circ$ ; (d)  $140^\circ$ ; (e)  $160^\circ$ . Symbols correspond to the following type of calculation: CASPT2 ( $\circ$ ) and CASSCF ( $\bullet$ ). See the text.

### C. CASPT2 study of the entrance zone

We have performed a study of the potential energy curves for the approximation of  $O(^1D)$  to  $N_2O$  in which a dense grid of points and several angles of approach were found necessary in order to gain deeper insight into the structure of this very important zone. In Figs. 4 and 5 plots of the energy calculated at the CASSCF(14,12) and CASPT2//CASSCF(14,12) levels in front of the attack distance for several angles of approach and for reactions (1) and (2), respectively, are presented. As a first approximation, the  $N_2O$  distances were kept fixed at the optimal equilibrium CASSCF(14,12) values. We note that the weight of the CASSCF reference wave function in the CASPT2 one had to be maintained almost constant in order to obtain smooth energy curves. We have done so by using the imaginary shift technique,<sup>58-60</sup> as implemented in the MOLCAS 4.1 program, thus correcting for the differences in reference weight for the set of geometries considered. In Figs. 4 and 5 one can notice the dramatic change in the shape of the potential energy surface when comparing CASSCF with CASPT2 results. The vdW minimum and the TS CASSCF geometries are considerably shifted and the possible reaction barrier is now placed below reactants for reaction (1), and turns into an inflection point for reaction (2) (not appreciated in the scale of Fig. 5). The angle giving the lowest-energy profile is about  $120^\circ$  in reaction (1), which is near the O–NNO angle at TS A1 as

determined at the CASSCF(14,12) level, and about  $100^\circ$  in reaction (2), near the O–ONN angle at TS A2 and at the same level. In Fig. 6 the minimum energy paths were obtained by fixing the attacking O–NNO distance [reaction (1)] or the attacking O–ONN distance [reaction (2)] and optimizing the rest of parameters at the CASSCF(14,12) level (always in  $C_s$  symmetry); point-wise CASPT2 calculations were then performed on the resulting geometries. The curves are very similar to those obtained at fixed geometries for the near-optimal angles of approach, thus indicating that freezing the NNO moiety does not introduce an important error in the paths at fixed angle. We have also used an analytical LEPS empirical PES previously derived in our group<sup>22</sup> assuming a pseudotriatomic model. As one can see, the LEPS energy profiles for reaction (1) are similar and tend to converge to the CASPT2 ones as the oxygen atom approaches the  $N_2O$  molecule, though they are considerably more attractive in the entrance zone.

### IV. RATE CONSTANTS

Rate constant calculations based on the conventional transition state theory (TST)<sup>61</sup> require the structure, harmonic vibrational frequencies, and energy of the TSs. The geometry of the TSs was determined by means of local fits around the geometries obtained in the minimum energy paths, and considering the  $N_2O$  as a frozen fragment with its

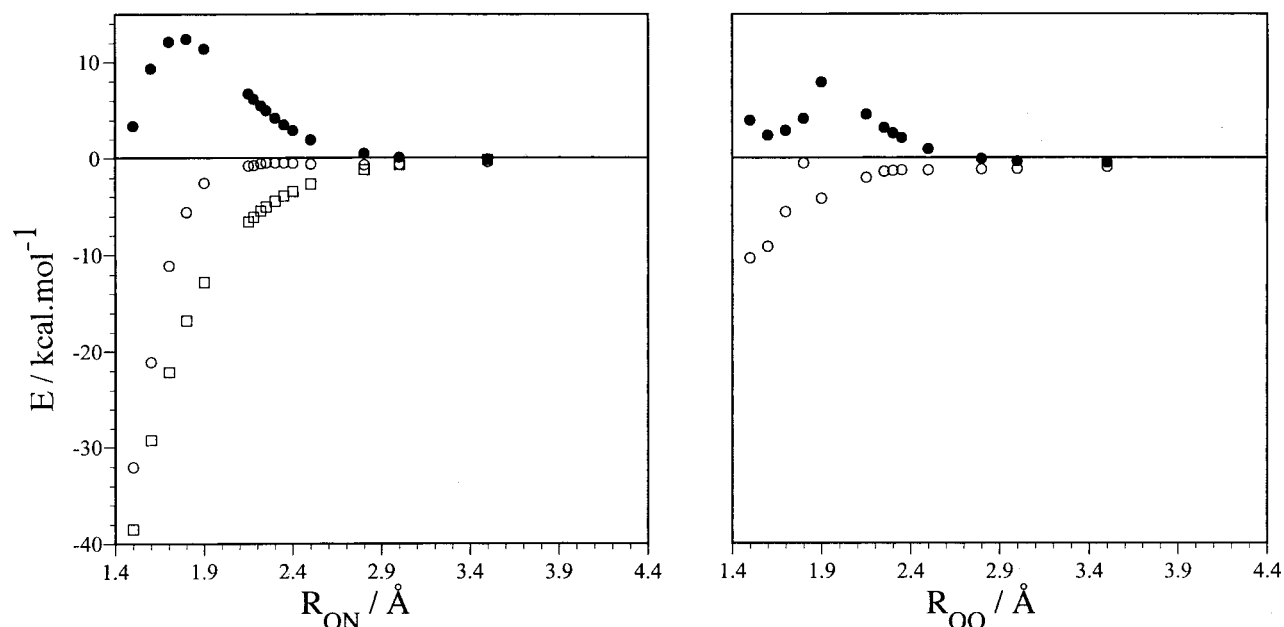


FIG. 6. Minimum energy path with energy relative to reactants, O(<sup>1</sup>D)+N<sub>2</sub>O, for: (left) reaction (1); (right) reaction (2). Symbols correspond to the following types of calculation: CASPT2 (○), CASSCF (●), and LEPS empirical surface (□). See the text.

own frequencies. For reaction (1) a bidimensional grid in the O–NNO distance and angle was fitted to a bicubic spline polynomial expression, taking the other parameters as those optimal at the CASSCF level. The fit was then used to deduce the corresponding harmonic vibrational frequencies for these degrees of freedom. For reaction (2) we have made the assumption that a TS exists and that it is located nearby the inflection point commented on above. In the same way a one-dimensional fourth-degree polynomial fit in the O–ONN angle was performed, and the frequency was also deduced. We did not try to determine the imaginary frequency of this TS because we do not need it for the subsequent calculations. The geometry, frequencies, and energy of both TSs are given in Table VI. Note that the  $R_{ON}$  and  $R_{OO}$  distances are remarkably longer than for CASSCF(18,14) TS A1 and TS A2 structures in Table II. This is a consequence of the importance of dynamical correlation in this system, as indicated above.

With this set of data it is possible to estimate the rate constants of reaction at different temperatures as well as the branching ratio between both reactions, and to compare them with experimental data. To this aim, we have performed con-

ventional TST rate constant calculations assuming that the reactivity is dominated by the CASPT2(14,12) entrance channel transition states reported in Sec. III C. We recall that in  $C_s$  symmetry two PESs ( $1^1A'$  and  $1^1A''$ ) correlate with the reactants and products of reactions (1) and (2). Hence, the total rate constant for reaction (1) can be expressed as

$$k_1 = k_1(1^1A') + k_1(1^1A''), \quad (4a)$$

and an analogous expression can be written for reaction (2), i.e.,

$$k_2 = k_2(1^1A') + k_2(1^1A''). \quad (4b)$$

According to Eqs. (4a) and (4b), we need further information regarding the  $1^1A''$  PES. For both reactions (1) and (2) we have located the corresponding TSs for the *cis*- and *trans*-arrangements, the computed barrier heights being 2.4 and 5.3 kcal mol<sup>-1</sup> for reaction (1) and 11.5 and 25.2 kcal mol<sup>-1</sup> for reaction (2), respectively [values obtained at the CASPT2//CASSCF(18,14) level including the CASSCF(14,12) ZPE]. Their geometrical parameters are detailed in Ref. 62, while more details on the  $1^1A''$  are cur-

TABLE VI. CASPT2(14,12) entrance transition states for reactions (1) and (2).

	Geometry (Å, °) <sup>a,b</sup>					E/kcal.mol <sup>-1</sup> <sup>d</sup>	ω <sub>i</sub> /cm <sup>-1</sup> <sup>e</sup>			
	$R_{NN}$	$R_{NO}$	$R_{OO}$	<NNO	<NOO		Dihedral <sup>c</sup>			
Reaction (1) TS	1.1329	1.1883, 2.3260		180.0, 109.1		180.0	-0.6	2275.2( <i>a'</i> ) 10.4( <i>a'</i> )	1296.2( <i>a'</i> ) 165.2( <i>i(a')</i> )	603.0( <i>a'</i> ) 603.0( <i>a''</i> )
Reaction (2) TS	1.1310	1.1926	2.35	180.0	98.9	180.0	-1.5	2275.2( <i>a'</i> ) 13.9( <i>a'</i> )	1296.2( <i>a'</i> )	603.0( <i>a'</i> ) 603.0( <i>a''</i> )

<sup>a</sup>Second  $R_{NO}$  distance and <NNO angle for reaction (1) TS and <NOO for reaction (2) TS calculated by means of fits to grids of points (see the text).

<sup>b</sup>The principal moments of inertia (in a.u.) for these two transition states are as follows:  $9.26 \times 10^5$ (*C*),  $8.06 \times 10^5$ (*B*),  $1.20 \times 10^5$ (*A*) [reaction (1) TS]; and  $8.43 \times 10^5$ (*C*),  $6.84 \times 10^5$ (*B*),  $1.58 \times 10^5$ (*A*) [reaction (2) TS], where the molecular symmetry plane has been taken as the *BC* one.

<sup>c</sup>Dihedral angle is defined as <ONNO for reaction (1) and <NNOO for reaction (2).

<sup>d</sup>Energies relative to reactants O(<sup>1</sup>D)+N<sub>2</sub>O at the same level.

<sup>e</sup>Last two frequencies for reaction (1) TS and last frequency for reaction (2) TS calculated by means of fits to grids of points (see the text).

rently being investigated. The barrier heights for the  $1^1A''$  TSs imply a negligible contribution to the total rate constant in the range of temperatures considered. Therefore, in what follows only the  $1^1A'$  PES will be taken into account.

The electronic partition function ratio for each of the TSs on the  $1^1A'$  PES is given by

$$\frac{z_{\text{el,TS}}}{z_{\text{el,O}} z_{\text{el,N}_2\text{O}}} = \frac{1}{5}. \quad (5)$$

Tunneling corrections are expected to be very low, owned to the negligible barrier heights and the atoms being relatively heavy, and have not been considered. For reaction (1), a comparison has also been made with the rate constants obtained by using the above-mentioned LEPS PES and running quasiclassical trajectories<sup>63</sup> on it using the TRIQCT program.<sup>64</sup> A set of 10 000 trajectories for each temperature was deemed sufficient for the present purpose of calculating rate constants, since a low statistical uncertainty was achieved. A number of reactive trajectories of between 1700 and 3000 was obtained within the range of temperatures studied. Under the reasonable assumption that reactivity in the temperature range explored is dominated by the ground PES ( $1^1A'$ ), we have taken the QCT rate constant for reaction

TABLE VII. Rate constants (in  $\text{cm}^{-3} \text{molecule}^{-1} \text{s}^{-1}$ ). Experimental data (Ref. 3):  $k_1 = 7.2(+3.0, -2.1) \times 10^{-11}$ ,  $k_2 = 4.4(+1.8, -1.3) \times 10^{-11}$ , and  $k_1/k_2 = 1.6(+1.7, -0.8)$  for  $T: 200\text{--}350 \text{ K}$ .

T/K	$k_1 \times 10^{11}$		$k_2 \times 10^{11}$		$k_1/k_2$
	TST (CASPT2)	QCT (LEPS) <sup>a</sup>	TST (CASPT2)	TST (CASPT2)	
100	4.29	3.42±0.04	1.54	2.79	
150	4.88	3.63±0.06	2.25	2.17	
200	5.67	3.74±0.06	2.95	1.92	
250	6.53	3.86±0.07	3.66	1.78	
300	7.42	3.92±0.07	4.36	1.70	
350	8.32	4.18±0.07	5.06	1.64	
400	9.23	4.30±0.07	5.77	1.60	
450	10.2	4.40±0.08	6.48	1.57	
500	11.1	4.48±0.08	7.18	1.54	
550	12.0	4.63±0.09	7.88	1.52	
600	12.9	4.62±0.09	8.59	1.50	
750	15.7	5.04±0.10	10.7	1.47	
1000	20.4	5.30±0.10	14.2	1.44	

<sup>a</sup>The statistical error (one standard deviation) is indicated.

(1) as the one resulting from the QCT calculation on the  $1^1A'$  PES divided by 5 (electronic degeneracy in reactants).

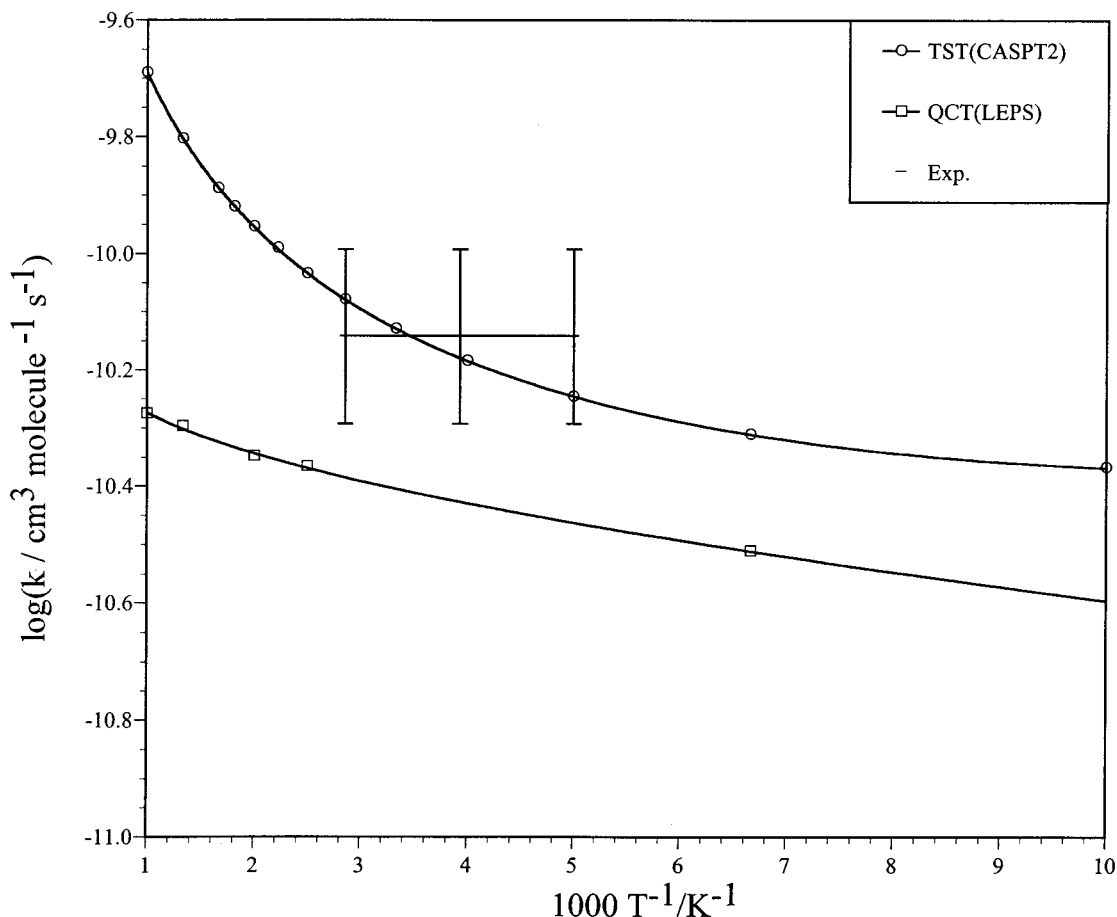


FIG. 7. Arrhenius plot of the rate constant for reaction (1) within the 100–1000 K range of temperatures, taking into account the TST(CASPT2), QCT(LEPS), and experimental (Ref. 3) results. The curves shown correspond to fits of the TST and QCT rate constants based on the expression  $k(T) = AT^n \times \exp(-E_0/RT)$ :  $A = 1.90 \times 10^{-13}$ ,  $n = 9.99 \times 10^{-1}$ ,  $E_0/R = -8.22 \times 10^1$  for TST(CASPT2), and  $A = 7.84 \times 10^{-12}$ ,  $n = 2.74 \times 10^{-1}$ ,  $E_0/R = -2.37 \times 10^1$  for QCT(LEPS).

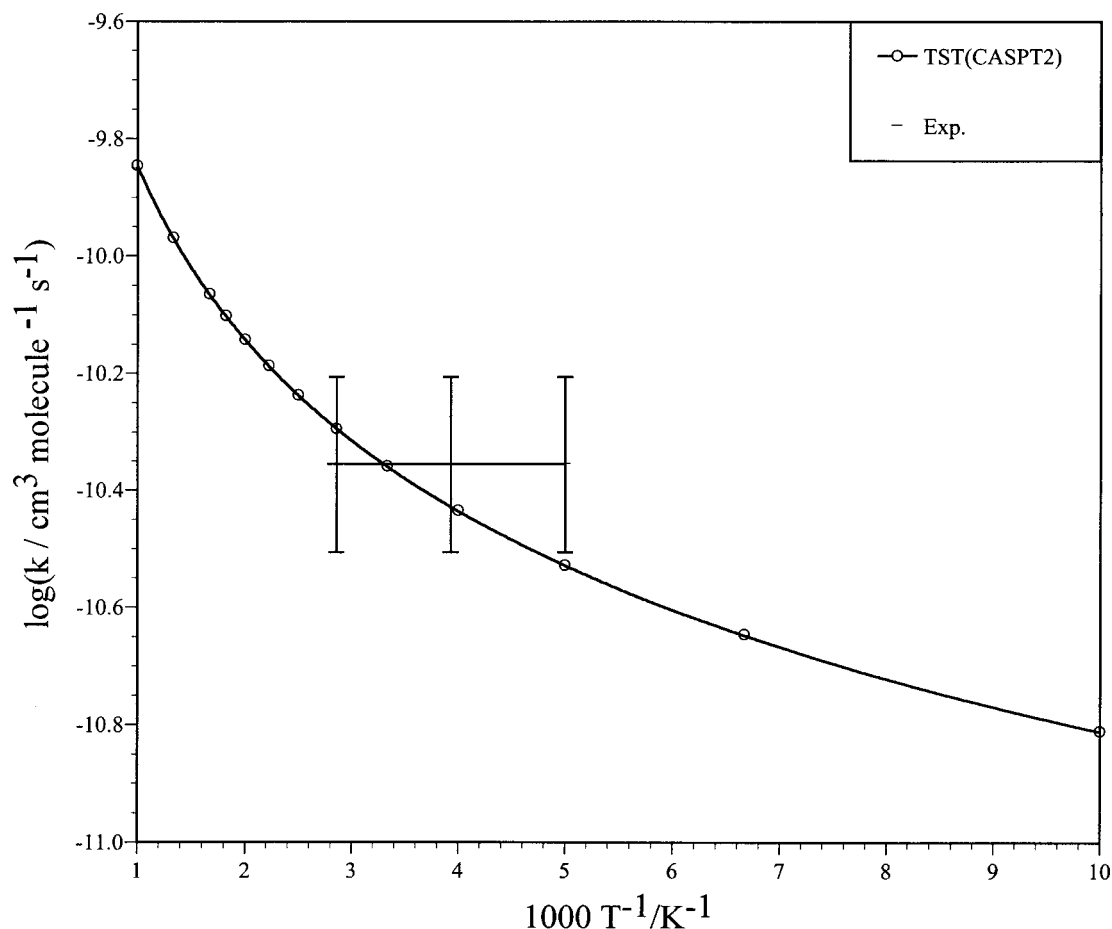


FIG. 8. Arrhenius plot of the rate constant for reaction (2) within the 100–1000 K range of temperatures, taking into account the TST(CASPT2) and experimental (Ref. 3) results. The curve shown corresponds to a fit of the TST rate constant values based on the expression  $k(T) = AT^n \exp(-E_0/RT)$ :  $A = 1.45 \times 10^{-13}$ ,  $n = 9.96 \times 10^{-1}$ ,  $E_0/R = -7.85$ .

On the other hand, the TST theory cannot be applied to the LEPS potential surface because of the absence of any TS.

The values of the rate constants in front of temperature are given in Table VII. In the CASPT2 case almost-perfect agreement with experiment was found by taking the height of the classical barrier (i.e., that derived without taking into account the ZPE energies of reactants and TSs) simply as an adjustable parameter at a temperature of 300 K. The optimal values obtained are around  $-0.15 \text{ kcal mol}^{-1}$  for reaction (1) and around  $0.0 \text{ kcal mol}^{-1}$  for reaction (2). If the classical barrier height for reaction (1) is also taken as zero, the computed rate constants increase slightly, although their values are still within the experimental error bounds. In Table VII one can notice the slight variation in the rate constants for this range of temperatures, in accordance with experiment. This is particularly true for the LEPS PES (QCT calculation), but also for the CASPT2 TST results if we restrict ourselves to the experimentally studied range, i.e., 200–350 K. Within this temperature interval the CASPT2 TST rate constants are within the experimental error bounds for both reactions. Arrhenius plots of the CASPT2 TST and LEPS QCT derived results are presented in Figs. 7 and 8, and the CASPT2 TST branching ratio is given in Fig. 9. A very good fit of the data was obtained by using an expression of the kind  $k(T) = AT^n \exp(-E_0/RT)$ . The expressions for each fit are given

in the captions of the figures. Notice the nonlinearity of the plots (non-Arrhenian behavior of the system). The branching ratio is somewhat higher than the experimental one but still in good agreement with it (Fig. 9), and the slope of the plot decreases with increasing temperature. We finally note the rather large uncertainty in the experimental rate constants and branching ratio.

## V. SUMMARY AND CONCLUSIONS

An *ab initio* study of the  $^1A'$  ground PES of the  $O(^1D) + N_2O(X^1\Sigma^+)$  reaction has been performed mainly at the CASPT2//CASSCF level. The stationary points of the two fast reactions leading to  $2 \text{ NO}(X^2\Pi)$  and  $N_2(X^1\Sigma_g^+) + O_2(a^1\Delta_g)$  products have been located and characterized as either minima or transition states calculating their harmonic vibrational frequencies. Two paths are found to be feasible in reaction (1), i.e., those bearing predominant *trans*- and *cis*-arrangements, the *trans*- one connecting directly with reactants. A rather complicated dynamics would thus be expected for this reaction, which is the most amenable for comparison with experimental studies. In reaction (2) several structures are found in the entrance zone of the reaction. Some of them would possibly not be obtained if full

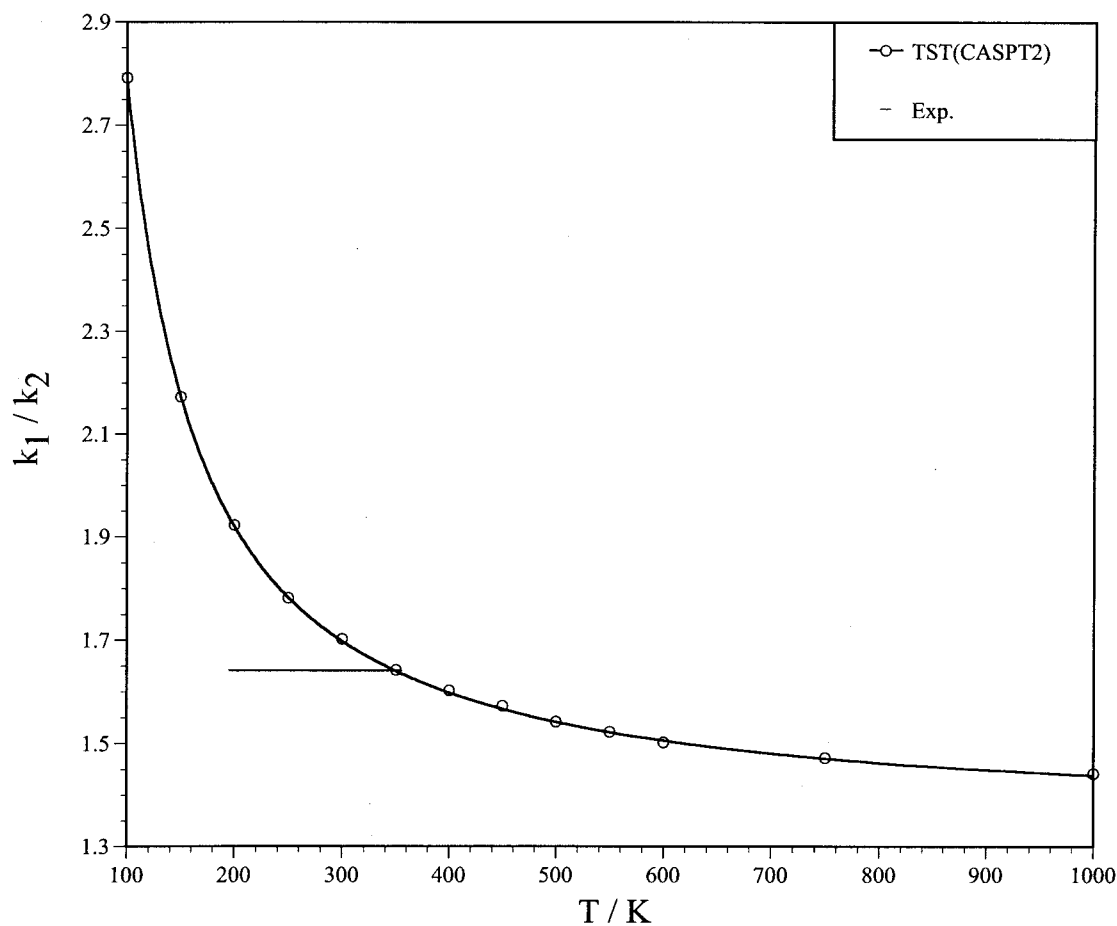


FIG. 9. Plot of the  $k_1/k_2$  rate constants ratio within the 100–1000 K range of temperatures, taking into account the TST(CASPT2) and experimental (Ref. 3) results. The curve shows the results obtained from a fit of the TST rate constants ratio based on the expression  $k(T) = AT^n \exp(-E_0/RT)$  for each rate constant:  $A_1/A_2 = 1.24$ ,  $\Delta n = 9.96 \times 10^{-3}$ ,  $\Delta E_0/R = -7.62 \times 10^1$ . Experimental error bounds are not indicated since they would exceed the bounds of the figure.

optimization at the CASPT2 level were performed. Most remarkable is the decrease in energy observed when introducing dynamical correlation to the system using the CASPT2 method in the form of point-wise calculations. This suggests that CASSCF energies are not very meaningful, even if some of the structures are reasonably well predicted. Regarding this, we note the considerable shift produced in the geometries of the stationary points located in the very entrance and exit zones when a more thorough CASPT2 study of these zones is carried out. We should stress the difficulty of obtaining accurate enough parameters for the TSs determining the rate constants, given the practical absence of barriers for both reactions, as suggested by the experimental data. A successful TST rate constant calculation based on these TSs could finally be achieved, reaching an almost quantitative agreement with experiment, particularly if the barrier heights are taken as adjustable parameters. Results obtained from QCT calculations on an analytical LEPS empirical PES for reaction (1) previously developed by our group are also in good accord with experiment. This agreement seems reasonable since the shape of the CASPT2 and LEPS PESs is similar.

We expect to undertake in the near future a dynamical study of this reaction, based on an analytical fit of the *ab*

*initio* information derived in this work, to obtain deeper insight into this important atmospheric reaction.

## ACKNOWLEDGMENTS

This work has been supported by the Spanish Ministry of Education and Culture through the DGES project No. PB98-1209-C02-01. Financial support from the “Generalitat de Catalunya” (Autonomous Government of Catalonia) Refs. Nos. 1998SGR 00008 and 2000SGR 00016 is also acknowledged. One of the authors (R.V.) also thanks the “Generalitat de Catalunya” for a “Beca de Formació d’Investigadors” Research Grant. The authors are also grateful to the “Centre de Supercomputació i Comunicacions de Catalunya (C<sup>4</sup>-CESCA/CEPBA)” for computer time made available.

<sup>1</sup>P. Warneck, *Chemistry of the Natural Atmosphere* (Academic, San Diego, 1988).

<sup>2</sup>M. W. Chase, Jr., C. A. Davies, J. R. Downey, Jr., D. J. Frurip, R. A. McDonald, and A. N. Syverud, *J. Phys. Chem. Ref. Data Suppl.* **14**, 1 (1985).

<sup>3</sup>R. Atkinson, D. L. Baulch, R. A. Cox, R. F. Hampson, Jr., J. A. Kerr, and J. Troe, *J. Phys. Chem. Ref. Data* **21**, 1125 (1992).

<sup>4</sup>G. A. Chamberlain and J. P. Simons, *J. Chem. Soc., Faraday Trans. 2* **71**, 402 (1975).

<sup>5</sup>P. A. Enríquez, Ph.D. thesis (Nottingham, 1993).

- <sup>6</sup>X. Wang, H. Li, Q. Zhu, F. Kong, and H. Yu, *J. Chin. Chem. Soc. (Taipei)* **42**, 399 (1995).
- <sup>7</sup>H. Akagi, Y. Fujimura, and O. Kajimoto, *J. Chem. Soc., Faraday Trans.* **94**, 1575 (1998).
- <sup>8</sup>M. Brouard, S. P. Duxon, P. A. Enríquez, and J. P. Simons, *J. Chem. Phys.* **97**, 7414 (1992).
- <sup>9</sup>S. P. Duxon, Ph.D. thesis (Nottingham, 1993).
- <sup>10</sup>H. Akagi, Y. Fujimura, and O. Kajimoto, *J. Chem. Phys.* **111**, 115 (1999).
- <sup>11</sup>P. J. Pisano, M. S. Westley, and P. L. Houston, *Chem. Phys. Lett.* **318**, 385 (2000).
- <sup>12</sup>M. Brouard, S. P. Duxon, P. A. Enríquez, R. Sayós, and J. P. Simons, *J. Phys. Chem.* **95**, 8169 (1991).
- <sup>13</sup>H. Tsurumaki, Y. Fujimura, and O. Kajimoto, *J. Chem. Phys.* **111**, 592 (1999).
- <sup>14</sup>M. Brouard and J. P. Simons, in *The Chemical Dynamics and Kinetics of Small Radicals*, edited by K. Liu and A. Wagner (World Scientific, Singapore, 1995), Part II, p. 795.
- <sup>15</sup>K. Honma, Y. Fujimura, O. Kajimoto, and G. Inoue, *J. Chem. Phys.* **88**, 4739 (1988).
- <sup>16</sup>I. Last, A. Aguilar, R. Sayós, M. González, and M. Gilibert, *J. Phys. Chem. A* **101**, 1206 (1997).
- <sup>17</sup>M. A. Vincent, I. H. Hillier, and L. Salsi, *Phys. Chem. Chem. Phys.* **2**, 707 (2000).
- <sup>18</sup>R. Valero, Tesis de Licenciatura, University of Barcelona (1997).
- <sup>19</sup>H. Akagi, A. Yokoyama, Y. Fujimura, and T. Takayanagi, *Chem. Phys. Lett.* **324**, 423 (2000).
- <sup>20</sup>M. Ben-Nun, M. Brouard, J. P. Simons, and R. D. Levine, *Chem. Phys. Lett.* **210**, 423 (1993).
- <sup>21</sup>M. González, R. Sayós, P. A. Enríquez, D. Troya, and M. P. Puyuelo, *Faraday Discuss.* **108**, 449 (1997).
- <sup>22</sup>M. González, D. Troya, M. P. Puyuelo, R. Sayós, and P. Enríquez, *Chem. Phys. Lett.* **300**, 603 (1999).
- <sup>23</sup>H. Yu, J. Cheng, and Z. Zhu, *J. Chem. Phys.* **7**, 124 (1994).
- <sup>24</sup>R. González-Luque, M. Merchán, and B. O. Roos, *Theor. Chim. Acta* **88**, 425 (1994).
- <sup>25</sup>R. Sayós, R. Valero, J. M. Anglada, and M. González, *J. Chem. Phys.* **112**, 6608 (2000), and references therein.
- <sup>26</sup>B. S. Jursic and Z. Zdravkovski, *Int. J. Quantum Chem.* **54**, 161 (1995).
- <sup>27</sup>H. A. Duarte, E. Proynov, and D. R. Salahub, *J. Chem. Phys.* **109**, 26 (1998).
- <sup>28</sup>A. R. W. McKellar, J. K. G. Watson, and B. J. Howard, *Mol. Phys.* **86**, 273 (1995).
- <sup>29</sup>A. Dkhissi, P. Soulard, A. Perrin, and N. Lacome, *J. Mol. Spectrosc.* **183**, 12 (1997).
- <sup>30</sup>A. L. L. East, A. R. W. McKellar, and J. K. G. Watson, *J. Chem. Phys.* **109**, 4378 (1998).
- <sup>31</sup>L. Krim and N. Lacome, *J. Phys. Chem. A* **102**, 2289 (1998).
- <sup>32</sup>F. Legay and N. Legay-Sommaire, *Chem. Phys. Lett.* **211**, 516 (1993).
- <sup>33</sup>H. H. Michels and J. A. Montgomery, Jr., *J. Chem. Phys.* **88**, 7248 (1988).
- <sup>34</sup>K. A. Nguyen, M. S. Gordon, J. A. Montgomery, Jr., H. H. Michels, and D. R. Yarkony, *J. Chem. Phys.* **98**, 3845 (1993).
- <sup>35</sup>K. A. Nguyen, M. S. Gordon, J. A. Montgomery, Jr., and H. H. Michels, *J. Phys. Chem.* **98**, 10072 (1994).
- <sup>36</sup>K. A. Nguyen, M. S. Gordon, and J. A. Boatz, *J. Am. Chem. Soc.* **116**, 9241 (1994).
- <sup>37</sup>G. Chaban, M. S. Gordon, and K. A. Nguyen, *J. Phys. Chem. A* **101**, 4283 (1997).
- <sup>38</sup>J. M. Mercero, X. Lopez, J. E. Fowler, and J. Ugalde, *J. Phys. Chem. A* **101**, 5574 (1997).
- <sup>39</sup>L. Salem and C. Rowland, *Angew. Chem. Int. Ed. Engl.* **11**, 92 (1972).
- <sup>40</sup>M. J. Frisch, G. W. Trucks, M. Head-Gordon, *et al.* GAUSSIAN 94, Revision B3, Gaussian, Inc., Pittsburgh, PA (1994).
- <sup>41</sup>L. Noodleman and D. A. Case, *Adv. Inorg. Chem.* **38**, 423 (1992).
- <sup>42</sup>K. Yamaguchi, F. Jensen, A. Dorigo, and K. N. Houk, *Chem. Phys. Lett.* **149**, 537 (1988).
- <sup>43</sup>B. O. Roos, *Adv. Chem. Phys.* **69**, 399 (1987).
- <sup>44</sup>K. Andersson and B. O. Roos, *Int. J. Quantum Chem.* **45**, 591 (1993).
- <sup>45</sup>K. Andersson and B. O. Roos, in *Modern Electronic Structure Theory*, edited by D. R. Yarkony (World Scientific, Singapore, 1995), Part I, p. 55.
- <sup>46</sup>P. C. Hariharan and J. A. Pople, *Theor. Chim. Acta* **28**, 213 (1973).
- <sup>47</sup>R. Krishnan, J. S. Binkley, R. Seeger, and J. A. Pople, *J. Chem. Phys.* **72**, 650 (1980).
- <sup>48</sup>M. J. Frisch, J. A. Pople, and J. S. Binkley, *J. Chem. Phys.* **80**, 3265 (1984).
- <sup>49</sup>MOLCAS Version 4.1, K. Andersson, M. R. A. Blomberg, M. P. Fülscher, *et al.*, Lund University, Sweden (1998).
- <sup>50</sup>P. Pulay and T. P. Hamilton, *J. Chem. Phys.* **88**, 4926 (1988).
- <sup>51</sup>J. M. Anglada and J. M. Bofill, *Chem. Phys. Lett.* **243**, 151 (1995).
- <sup>52</sup>M. W. Schmidt and M. S. Gordon, *Annu. Rev. Phys. Chem.* **49**, 233 (1998).
- <sup>53</sup>R. Shepard, *Adv. Chem. Phys.* **69**, 63 (1987).
- <sup>54</sup>S. Bashkin and J. O. Stoner, Jr., *Atomic Energy Levels and Grottrian Diagrams* (North-Holland, Amsterdam, 1975), Vol. 1.
- <sup>55</sup>K. P. Huber and G. Herzberg, *Molecular Spectra and Molecular Structure*, Vol. 4, *Constants of Diatomic Molecules* (Van-Nostrand Reinhold, New York, 1979).
- <sup>56</sup>H. Okabe, *Photochemistry of Small Molecules* (Wiley, New York, 1978).
- <sup>57</sup>J.-L. Teffo and A. Chédin, *J. Mol. Spectrosc.* **135**, 389 (1989).
- <sup>58</sup>B. O. Roos and K. Andersson, *Chem. Phys. Lett.* **245**, 215 (1995).
- <sup>59</sup>B. O. Roos, K. Andersson, M. P. Fülscher, L. Serrano-Andrés, K. Pierloot, M. Merchán, and V. Molina, *J. Mol. Struct.: THEOCHEM* **388**, 257 (1996).
- <sup>60</sup>N. Forsberg and P.-A. Malmqvist, *Chem. Phys. Lett.* **274**, 196 (1997).
- <sup>61</sup>D. G. Truhlar, A. D. Isaacson, and B. C. Garrett, in *Theory of Chemical Reaction Dynamics*, edited by M. Baer (CRC, Boca Raton, 1985), vol. 4, p. 65.
- <sup>62</sup>The geometries of the <sup>1</sup>A'' entrance channel TSs at the CASSCF(18,14) level are as follows: Reaction (1) O–N–N'–O' geometry; *cis*-TS:  $R_{NN'} = 1.18 \text{ \AA}$ ,  $R_{N'O'} = 1.20 \text{ \AA}$ ,  $R_{ON} = 1.84 \text{ \AA}$ ,  $\angle NN'O' = 160.0^\circ$ ,  $\angle ONN' = 107.0^\circ$ , *trans*-TS:  $R_{NN'} = 1.18 \text{ \AA}$ ,  $R_{N'O'} = 1.20 \text{ \AA}$ ,  $R_{ON} = 1.79 \text{ \AA}$ ,  $\angle NN'O' = 160.0^\circ$ ,  $\angle ONN' = 106.0^\circ$ . Reaction (2) (N–N'–O'–O geometry): *cis*-TS:  $R_{NN'} = 1.17 \text{ \AA}$ ,  $R_{N'O'} = 1.28 \text{ \AA}$ ,  $R_{OO'} = 1.87 \text{ \AA}$ ,  $\angle NN'O' = 145.0^\circ$ ,  $\angle N'O'O = 113.0^\circ$ ; *trans*-TS:  $R_{NN'} = 1.21 \text{ \AA}$ ,  $R_{N'O'} = 1.21 \text{ \AA}$ ,  $R_{ON} = 2.03 \text{ \AA}$ ,  $\angle NN'O' = 140.0^\circ$ ,  $\angle N'O'O = 111.0^\circ$ .
- <sup>63</sup>H. R. Mayne, *Int. Rev. Phys. Chem.* **10**, 107 (1991).
- <sup>64</sup>R. Sayós and M. González, TRIQCT, unpublished program.